



**NAVAL
POSTGRADUATE
SCHOOL**

MONTEREY, CALIFORNIA

THESIS

**WIND TUNNEL RENOVATION, FLOW VERIFICATION
AND FLAPPING WING ANALYSIS**

by

Curtis Hickle

June 2006

Thesis Advisor:
Second Reader:

Kevin Jones
Garth Hobson

Approved for public release; distribution is unlimited

THIS PAGE INTENTIONALLY LEFT BLANK

REPORT DOCUMENTATION PAGE			Form Approved OMB No. 0704-0188	
Public reporting burden for this collection of information is estimated to average 1 hour per response, including the time for reviewing instruction, searching existing data sources, gathering and maintaining the data needed, and completing and reviewing the collection of information. Send comments regarding this burden estimate or any other aspect of this collection of information, including suggestions for reducing this burden, to Washington headquarters Services, Directorate for Information Operations and Reports, 1215 Jefferson Davis Highway, Suite 1204, Arlington, VA 22202-4302, and to the Office of Management and Budget, Paperwork Reduction Project (0704-0188) Washington DC 20503.				
1. AGENCY USE ONLY (Leave blank)		2. REPORT DATE June 2006	3. REPORT TYPE AND DATES COVERED Master's Thesis	
4. TITLE AND SUBTITLE: Wind Tunnel Renovation, Flow Verification and Flapping Wing Analysis.			5. FUNDING NUMBERS	
6. AUTHOR(S) Curtis James Hickle				
7. PERFORMING ORGANIZATION NAME(S) AND ADDRESS(ES) Naval Postgraduate School Monterey, CA 93943-5000			8. PERFORMING ORGANIZATION REPORT NUMBER	
9. SPONSORING /MONITORING AGENCY NAME(S) AND ADDRESS(ES) N/A			10. SPONSORING/MONITORING AGENCY REPORT NUMBER	
11. SUPPLEMENTARY NOTES The views expressed in this thesis are those of the author and do not reflect the official policy or position of the Department of Defense or the U.S. Government.				
12a. DISTRIBUTION / AVAILABILITY STATEMENT Approved for public release; distribution is unlimited			12b. DISTRIBUTION CODE	
13. ABSTRACT (maximum 200 words) The Naval Postgraduate School (NPS) Micro-Air Vehicle (MAV) wind tunnel was refurbished in this study. This wind tunnel has a 61 by 38 centimeter test section with a contraction ratio of 6.75, and testing speeds up to 9 meters per second (m/s). The objectives of this work were to create a high quality, customized facility for further MAV study, and to fully characterize the wake of the MAV at a plane downstream of the model. Extensive repairs were made to the wind tunnel intake, test section, and fan. The flow field produced in the tunnel was analyzed with hot wire anemometry. The turbulence intensity ranged from .7% to .5% for freestream velocities of 2 m/s to 5 m/s. The velocity variation across the test section ranged from .251% to .125%. A model of the NPS MAV was placed in the test section and the wake was studied with and without the main wing, and in vertical and horizontal orientations. The wake was characterized with hot wire anemometry and flow visualization techniques at various flapping frequencies and freestream velocities.				
14. SUBJECT TERMS Low speed wind tunnel, Low Reynolds number, Constant temperature anemometry, Micro-Air Vehicle, Flapping wing.			15. NUMBER OF PAGES 95	
			16. PRICE CODE	
17. SECURITY CLASSIFICATION OF REPORT Unclassified	18. SECURITY CLASSIFICATION OF THIS PAGE Unclassified	19. SECURITY CLASSIFICATION OF ABSTRACT Unclassified	20. LIMITATION OF ABSTRACT UL	

THIS PAGE INTENTIONALLY LEFT BLANK

Approved for public release; distribution is unlimited

**WIND TUNNEL RENOVATION, FLOW VERIFICATION
AND FLAPPING WING ANALYSIS**

Curtis J. Hickle
Lieutenant Commander, United States Navy
B.S., University of Wisconsin, 1994
M.B.A., University of Rhode Island, 2002

Submitted in partial fulfillment of the
requirements for the degree of

MASTER OF SCIENCE IN MECHANICAL ENGINEERING

from the

**NAVAL POSTGRADUATE SCHOOL
June 2006**

Author: Curtis Hickle

Approved by: Dr. Kevin Jones
Thesis Advisor

Dr. Garth Hobson
Second Reader/Co-Advisor

Dr. Anthony Healy
Chairman, Department of Mechanical and Astronautical
Engineering

THIS PAGE INTENTIONALLY LEFT BLANK

ABSTRACT

The Naval Postgraduate School (NPS) Micro-Air Vehicle (MAV) wind tunnel was refurbished in this study. This wind tunnel has a 61 by 38 centimeter test section with a contraction ratio of 6.75, and testing speeds up to 9 meters per second (m/s). The objectives of this work were to create a high quality, customized facility for further MAV study, and to fully characterize the wake of the MAV at a plane downstream of the model. Extensive repairs were made to the wind tunnel intake, test section, and fan. The flow field produced in the tunnel was analyzed with hot wire anemometry. The turbulence intensity ranged from .7% to .5% for freestream velocities of 2 m/s to 5 m/s. The velocity variation across the test section ranged from .251% to .125%. A model of the NPS MAV was placed in the test section and the wake was studied with and without the main wing, and in vertical and horizontal orientations. The wake was characterized with hot wire anemometry and flow visualization techniques at various flapping frequencies and freestream velocities.

THIS PAGE INTENTIONALLY LEFT BLANK

TABLE OF CONTENTS

I.	INTRODUCTION.....	1
A.	BACKGROUND	1
B.	OBJECTIVE	1
C.	MAV CHALLENGES	2
1.	Low Reynolds Number Flight.....	2
2.	Additional Challenges.....	3
D.	THE NPS MAV	3
II.	RENOVATION.....	5
A.	OVERALL DESCRIPTION OF THE FLAWS.....	5
B.	WIND TUNNEL INTAKE.....	9
C.	TEST SECTION	10
D.	FAN	12
E.	MOTOR.....	17
F.	TRAVERSE MECHANISM.....	18
III.	EXPERIMENTAL SETUP	21
A.	WIND TUNNEL.....	21
1.	Description.....	21
B.	TRAVERSE MECHANISM	24
C.	CONSTANT TEMPERATURE ANEMOMETER	25
1.	Equipment Used.....	25
2.	Theory of Operation	25
D.	MAV MODEL	26
E.	PITOT TUBE FLOW REFERENCE	28
IV.	EXPERIMENTAL PROCEDURE AND RESULTS.....	29
A.	CALIBRATION.....	29
B.	FLOW VERIFICATION OF THE TUNNEL.....	29
1.	The Grid.....	29
2.	The Procedure	30
3.	Results at 2 m/s.....	30
4.	Results at 3 m/s.....	32
5.	Results at 5 m/s.....	34
C.	MODEL WAKE.....	35
1.	Flapping Wing Wake.....	35
2.	Wake Behind Complete Model.....	37
3.	Full Wake Characterization.....	40
D.	FLOW VISUALIZATION.....	43
V.	CONCLUSIONS	47
A.	TUNNEL FLOW VERIFICATION.....	47
B.	MODEL WAKE.....	47

C. RECOMMENDATIONS FOR FURTHER IMPROVEMENT	47
APPENDIX A. PITOT TUBE CALIBRATION.....	49
APPENDIX B. HOTWIRE CALIBRATION.....	51
APPENDIX C. FLOW VERIFICATION AT 2 M/S	53
APPENDIX D. FLOW VERIFICATION AT 3 M/S	57
APPENDIX E. FLOW VERIFICATION AT 5 M/S	61
APPENDIX F. FLAPPING WING WAKE AT CONSTANT Z POSITION.....	65
APPENDIX G. FULL MODEL WAKE AT 30 HZ AND 2 M/S	67
APPENDIX H. FULL MODEL WAKE AT 30 HZ AND 3 M/S	73
LIST OF REFERENCES	79
INITIAL DISTRIBUTION LIST	81

LIST OF FIGURES

Figure 1.	Wind Tunnel in Storage	5
Figure 2.	Exhaust Section in Storage	6
Figure 3.	Intake Section Damage	7
Figure 4.	Honeycomb Cells Blocked	7
Figure 5.	Test Section Access Hole and Felt on Floor Section	8
Figure 6.	Damaged Screen Section	10
Figure 7.	New Hinges.....	11
Figure 8.	Test Section Cut for Optical Quality Upgrade.....	11
Figure 9.	Holes in Frame for Floor Mounting.....	12
Figure 10.	Unbalanced Fan Hub.....	13
Figure 11.	Balanced Shaft	14
Figure 12.	Upper Fan Section.....	15
Figure 13.	Bearing Removal System.....	16
Figure 14.	Fully Assembled Fan Section	17
Figure 15.	Recessed Motor Mounting Plate.....	18
Figure 16.	Traverse Mechanism.....	19
Figure 17.	Traverse Mechanism Drive Belt	19
Figure 18.	Intake and Contraction Sections	23
Figure 19.	Contraction Contour [From REF 14].....	24
Figure 20.	Hotwire Measuring System [from REF 10].....	26
Figure 21.	NPS MAV Model [From REF 4].....	27
Figure 22.	Anemometer Probes.....	30
Figure 23.	Normalized Velocity at 2 m/s	31
Figure 24.	Turbulence Intensity at 2 m/s.....	32
Figure 25.	Normalized Velocity at 3 m/s	33
Figure 26.	Turbulence Intensity at 3 m/s.....	33
Figure 27.	Normalized Velocity at 5 m/s	34
Figure 28.	Turbulence Intensity at 5 m/s.....	35
Figure 29.	Vertical Model Without Main Wing.....	36
Figure 30.	Flapping Wing Wake at 20 Hz.....	37
Figure 31.	Flapping Wing Wake at 30 Hz.....	37
Figure 32.	Vertical Model With Main Wings	38
Figure 33.	Wake Behind Complete Model at 20 Hz	39
Figure 34.	Wake Behind Complete Model at 30 Hz	39
Figure 35.	Complete Horizontal Model in the Test Section.....	40
Figure 36.	Model Wake at 2 m/s	41
Figure 37.	Model Wake at 3 m/s	41
Figure 38.	Sketch of Vortex Structures [From REF 15]	42
Figure 39.	Main Wing Stalled When Not Flapping	44
Figure 40.	Flow Reattaches When Flapping	44
Figure 41.	Wingtip Vortex	45
Figure 42.	Wake Drawn Toward Centerline	45

THIS PAGE INTENTIONALLY LEFT BLANK

ACKNOWLEDGMENTS

The author would like to express his sincerest gratitude to Dr. Kevin Jones for his time and effort supervising and assisting in the completion of this project. His expertise in this field was essential. Additionally, the author would like to thank Dr. Garth Hobson for his oversight and encouragement.

Finally, the author would like to thank his family for their continuing support and encouragement throughout this process, without which this would not have been possible.

THIS PAGE INTENTIONALLY LEFT BLANK

I. INTRODUCTION

A. BACKGROUND

In the past, most military airborne surveillance missions were performed by expensive large piloted aircraft. Recent technological advances have led to the use of Unmanned Aerial Vehicles (UAVs) for reconnaissance tasks. UAVs are advantageous because they remove the human from the battlefield, are much smaller and less expensive, and are much stealthier than typical piloted aircraft. The next level of development will be in the area of Micro Air Vehicles (MAVs).

Real time satellite data, spy plane and UAV surveillance are becoming more accessible. However, the information provided from these sources is frequently not tailored to the small area detail required by lower level military leadership. The squad leader must still put troops in harm's way to scout over the next hill, through the alley or inside the next building. An effort is underway to change this. In 2000, the Defense Advanced Research Projects Agency (DARPA) set guidelines for the first generation of MAVs. Since then, major MAV competitions have taken place on national and international levels. Specifications and mission requirements vary, but the trend is clear: MAVs will play a significant role in future military action.

MAVs are especially advantageous in missions where human risk is involved. They could be used by government agencies involved in terrorist or hostage situations, search and rescue operations, environmental monitoring of smokestack emissions or chemical spills. Military missions such as video or infrared surveillance, battle damage assessment, weapon targeting, communications relay, detection of toxic gasses, radiation, or detection of land mines are also suited for MAV use.

B. OBJECTIVE

This project chronicles the rebuilding efforts of the Naval Postgraduate School (NPS) Micro Air Vehicle (MAV) wind tunnel, which will be used for MAV testing and

research. Extensive repairs were made resulting in a facility far superior to that used previously. The NPS low speed wind tunnel formerly used for MAV testing has been decommissioned and slated for removal. This facility had a number of flaws including a poor lip design and a close proximity to building walls and other articles that led to a turbulence intensity in excess of 2% at MAV velocities. It suffered from the ill effects of a short, rapid 9:1 ratio contraction and only one layer of screen in the intake with insufficient settling area. The details of the detriments of this construction will be developed further in subsequent chapters.

The goal of this work was to provide a viable facility for MAV testing and research. Additionally, this paper sought to analyze the flow around the NPS MAV using Constant Temperature Anemometry and flow visualization.

C. MAV CHALLENGES

1. Low Reynolds Number Flight

Because of their small size and low airspeed, MAVs operate at Reynolds numbers (Re) lower than conventional craft. One cannot simply scale down an existing aircraft to a six inch size and expect it to fly. Aerodynamic behavior is different in this low Re regime and has not been studied in depth. Most aircraft fly at Re in the millions, even 100 million for the largest commercial jets. At Re above 200,000 many simplifications can be made to the governing equations of flight to facilitate the design process. These simplifications are allowable because the flow around airfoils in this regime is dominated by inertial forces and can be modeled with vortex panel codes. At low Re, viscous effects play a larger role and can not be ignored. This required the use of Navier-Stokes based codes, which are more accurate, but also more time consuming and expensive. The NPS MAV operates at around Re 20,000 for the main wing and 5,000 for the flapping wings requiring these Navier-Stokes based methods.

Airfoil performance in the low Re regime is sensitive to separation. If the flow becomes separated from the airfoil, it will lose lift in a condition known as stall. Airfoils develop a pressure profile based on their shape and angle of attack. In general, the lowest

pressure develops on the top of an airfoil at a position 30% to 50% of the chord length known as the center of pressure (C_p). From the leading edge of the airfoil to this point the pressure gradient is from high pressure to low pressure known as favorable, or acting in the natural direction of the flow as the wing moves through the air. From the center of pressure to the trailing edge the gradient is unfavorable, or adverse, leading to potentially serious problems. An adverse pressure gradient tends to slow the flow as it moves from low pressure to high. Near the surface of the wing, the boundary layer has already reduced the momentum of the flow, so the adverse pressure gradient exacerbates the issue. The flow will gradually slow to zero velocity and even reverse direction. This recirculation flow is usually not attached to the surface of the wing and the flow is separated, or the airfoil is stalled. When stalled, the airfoil has dramatically reduced lift and the craft quickly loses altitude. This is a particularly dangerous condition for low flying vehicles like MAVs. At higher angles of attack, the pressure at the C_p decreases. This increases the adverse pressure gradient to the trailing edge and makes stall more likely. The NPS MAV handles the problem of stall with its unique design described in Part D below.

2. Additional Challenges

There are many other engineering challenges concerning possible MAV requirements. The vehicle must be lightweight and compact with flight stabilization necessary for low Re flow as outlined above. This requires the use of high energy density propulsion systems and high strength to weight ratio structural components. Lightweight, low power on board communication equipment must be integrated into the design with sufficient bandwidth for real time imaging. On board guidance, navigation and geolocation systems may also be desirable. The development of the sensors themselves will likely prove difficult as well.

D. THE NPS MAV

To meet these challenges the NPS MAV has taken an unconventional biomorphic approach. The craft consists of low aspect ratio wings flanking the fuselage followed by a pair of identical counterphase flapping wings. This allows the flapping wings to take

advantage of a phenomenon known as ground effect for increased performance. Ground effect is caused by the interruption of wingtip vortices. These vortices destroy large amounts of lift generated by the wing through increased downwash behind it. The symmetric action of the flapping wings interrupts these lift destroying vortices [REF 13]. This dual flapping wing design is also mechanically and aerodynamically balanced. A single wing system would be unbalanced and less efficient as the net torque on the main structure would induce undesired motion on the fuselage and main wing. Looking at the flow 2 dimensionally, a flapping wing sheds vortices at its tip adversely affecting its performance. However, for a pair of flapping wings, the image wing is positively affected by phenomenon enhancing the overall systems performance.

Another aerodynamic phenomenon the NPS MAV is uniquely suited to handle is the flow separation and stall problem at low Re flight mentioned above. The flapping wings produce a favorable pressure gradient in front of them and on the adjacent aft portion of the main wing. This suppresses flow separation and stall even in the low Re flight regime used by MAVs [REF 13].

The NPS MAV weighs around 12 grams and currently has no payload. It can fly between 2 and 5 m/s for a great degree of maneuverability. It currently does not have active pitch control, limiting the maximum safe speed.

II. RENOVATION

A. OVERALL DESCRIPTION OF THE FLAWS

The wind tunnel that would become the Naval Postgraduate School Micro Air Vehicle tunnel was discovered in a basement storage area as shown in figures 1 and 2.



Figure 1. Wind Tunnel in Storage



Figure 2. Exhaust Section in Storage

It was mostly complete but damaged in several sections and covered in a thick layer of dust. The dust itself was a flaw as dust always accumulates on the honeycomb and screens in irregular patterns which alters the flow [REF 1]. The honeycomb flow straightener material was damaged in several places, including a serious defect in the lower left corner of the intake (see Figure 3). The honeycomb was constructed of two separate sections. Several of the cells were blocked along the joint right through the center of the tunnel by the epoxy used to attach the two parts (See Figure 4). These blocked cells would have led to a disturbance in the test section flow [REF 1].



Figure 3. Intake Section Damage



Figure 4. Honeycomb Cells Blocked

There were numerous holes in various parts of the test section including a large hole in the side of the test section that was inaccurately sealed with a plug. There was a felt like material glued to the bottom of the test section. These defects are shown in Figure 4. All of these defects would have certainly disturbed the flow in the test section.

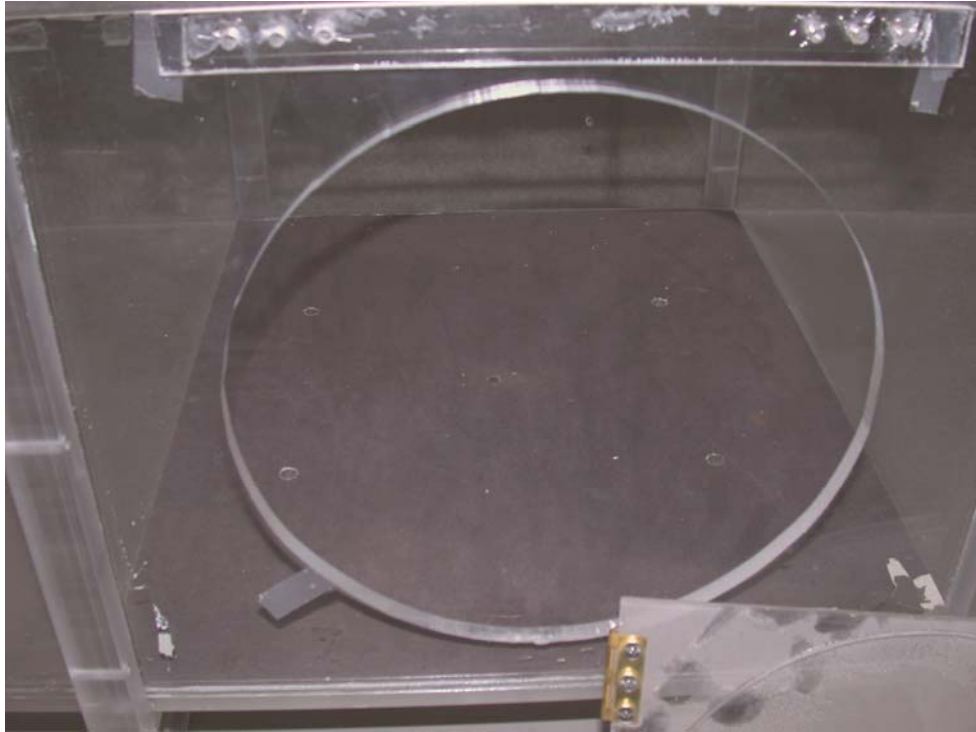


Figure 5. Test Section Access Hole and Felt on Floor Section

The motor used to drive the fan was a 1.5 hp General Electric AC motor. This device had limited speed control severely restricting its utility. To alter the tunnel flow speed the operator had to secure the flow, remove the stator, loosen the outer fan hub and adjust the fan blades before reassembling and checking the flow. The blades would have to be carefully aligned to the same pitch for aerodynamic balance and an even test section flow. This was an inaccurate and tedious method of adjusting the flow that proved unacceptable. More importantly, in short wind tunnels with relatively small contraction ratios such as this, the fan speed should be varied rather than the blade pitch to maintain an even velocity front in the test section [REF 1].

The tunnel also experienced significant vibration during operation that would limit its usefulness in MAV testing. This was caused by an unbalanced fan shaft. Vibrations must be limited because they adversely affect measuring systems, model operation, and flow visualization. Furthermore, vibrations can lead to transition and separated boundary layers.

A suitable location for the wind tunnel was found. When attempting to move the tunnel, it was discovered that the wheels had sunk into the asphalt floor. The intake section was raised with a hydraulic jack and plywood inserted under the wheels. Measurements were taken and it was discovered that the tunnel would not fit along the path to the new location. To accommodate the move, the intake section had to be disassembled. With this complete, the facility was moved to the new location.

B. WIND TUNNEL INTAKE

The wind tunnel intake was completely disassembled to facilitate moving the structure. The intake lip was attached to the structure with thirty-six bolts. The honeycomb and the layers of screen were held in place in individual wooden frames. The three frames were held together by thirty-two threaded rods with nuts on each end. The honeycomb flow straightener was judged to be beyond repair. It was carefully cut from its frame. The remaining epoxy was removed and the frame prepared with a belt sander. A replacement material was obtained but delivered with some damage. The corners were collapsed and a few areas in the center were slightly deformed. A heavy gauge wire was inserted into the cells to carefully reshape the material. The new honeycomb material was slightly collapsed with fine aluminum sheets to fit inside the frame. Then the honeycomb was permanently fixed to the frame by painstakingly applying epoxy around the interface.

One layer of the original screen was wired together from two separate sections of material and needed replacement as shown in Figure 6. This represented an improper splice that would have introduced turbulence into the flow [REF 1]. When an intake section is too large for a single section of screen, splicing must be done very carefully by

brazing individual wires together. When suitable replacement materials were obtained; the screen was replaced by pulling tight and stapling a single piece of appropriately sized screen over the frame.



Figure 6. Damaged Screen Section

C. TEST SECTION

The test section ceiling was mounted on failing hinges. New ones were obtained, holes drilled and tapped, and the top section was firmly attached to the rest of the structure as shown in Figure 7.



Figure 7. New Hinges

The felt material on the test section floor was removed with a commercial solvent and the area is shown clean in Figure 8. The large hole in the test section also required repair. New sheets of optical grade acrylic were obtained. This material was chosen to allow Laser Doppler Velocimetry measurements in future application. A large rectangular shape was removed from around the hole in the test section with a jigsaw as shown in Figure 8.



Figure 8. Test Section Cut for Optical Quality Upgrade

The area was carefully sanded until the new sheets could be inserted with a tight fit. Small strips of aluminum were obtained to support the pieces. Holes were drilled and tapped for mounting the aluminum strip to the tunnel and to the new sheet of material. It was cut to final size and a slot was added for flow measurement. Additional sheets have been prepared for easy replacement if necessary. A thin weatherstripping material was added at the joints to limit leakage. Large holes were cut in the framing of the tunnel to accommodate lighting or equipment mounting from the floor as shown in Figure 9.

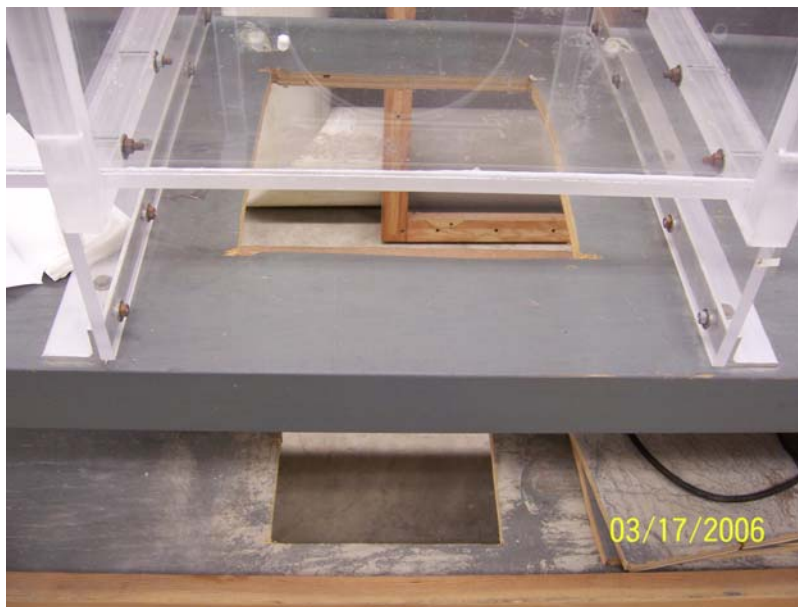


Figure 9. Holes in Frame for Floor Mounting

D. FAN

The tunnel vibrated excessively when operated. It was determined that the shaft and hub were out of balance. The fan section was removed for disassembly. Simple static balancing showed the structure to be significantly unbalanced. There were several holes drilled in the hub which contributed to the unbalanced condition as they appeared to be drilled on the light side of the hub (Figure 10). Three holes were drilled on the heavy side but were not having a significant effect. Weights were attached to the blades to

achieve balance and it was determined that simply drilling holes would not be enough to correct the situation. Some of the existing holes were filled with specially fabricated steel inserts and a weighted washer was constructed to bring the assembly in balance (Figure 11).



Figure 10. Unbalanced Fan Hub



Figure 11. Balanced Shaft

The fan was remounted with the tunnel completely assembled and tested. The fan stator would no longer fit with the addition of the balancing weight. One quarter inch of material was removed from the stator with a rotary tool and a cutoff wheel to allow full reassembly. Upon testing, the vibration was no longer present. However, while running at high speed the fan exhibited a grinding noise and the test run was halted. The shaft was difficult to turn by hand and the fan section was once again removed. It was determined that the bearings were failing. The shaft was supported by two ball bearing units under the hub and a flange bearing at the bottom of the fan section. In order to split the fan section the lower flange bearing had to be detached. The bearing was frozen on the shaft and proved difficult to remove. A specially modified two jaw gear puller was obtained. The ends of the extracting arms were sharpened on a grinder to fit in the small space between the bearing and the lower fan section. With extreme care, the tool successfully removed the bearing. This allowed separation of the lower fan section, after removing the bolts and prying it apart. At this point, the fan hub and blades required removal. The blades and corresponding sections of both halves of the hub were numbered to ensure the same balance upon installation, and the blade angles were marked to ensure the same aerodynamic balance. The bolts were removed and the modified gear

puller placed back in service to remove the outer fan hub section. With this removed, the blades were freely extracted. An additional gear puller was used to remove the inner fan hub and locating Woodruff key. The shaft was then extracted from the bottom of the upper fan section leaving the structure shown in Figure 12. This exposed the two ball bearing units, one on each end of the support shown in the middle of the photo. They proved difficult to remove as well.



Figure 12. Upper Fan Section

To remove and install the new ball bearing units, a pulling system was devised. This consisted of thick scrap aluminum, mill mounting pieces and a threaded rod. A piece of rectangular scrap was inserted into the bearing hole and righted. The threaded rod was then screwed into this piece which would apply force to the inside of the bearing. A thick section of scrap with a through hole for the threaded rod was inserted and balanced against the structure as shown in Figure 13. A nut was then threaded on the rod and turned to apply force to the inside of the bearing for removal. The bearing unit on the other end of the support was removed in this manner as well.



Figure 13. Bearing Removal System

Installation required similar tools. After new bearings were obtained, a longer rod was inserted through the whole support structure and threaded into a scrap piece on the other end. Then the same setup shown in Figure 13 was utilized except the support pieces contacted the new bearing. The nut was tightened and the bearing was pressed into place. The same action on the other end installed the opposing bearing.

The fan shaft was found to be corroding in several places. For this reason, it was placed in a lathe and polished for easier reassembly. The upper fan housing mating surface was left with epoxy residue as shown in Figure 12 above. This surface and the mating surface on the lower fan housing were prepared with a belt sander. Thin strips of weather-stripping material were added to ensure an air tight fit. The shaft was then inserted into two new bearings in the support housing. The inner fan hub was pressed into place and located with the key. The blades were reinstalled in their correct mounting holes and the outer hub was pressed into place in its corresponding position. The lower fan housing was then reattached and bolted together. The new flange bearing was added to the shaft and bolted to the lower fan housing. The coupling was added to the end of

the shaft and the completed fan housing was reattached to the wind tunnel structure, with additional weather-stripping inserted in the joint. The completed assembly is shown in Figure 14.



Figure 14. Fully Assembled Fan Section

E. MOTOR

An alternative driving force for the wind tunnel was sought to improve the control of the airflow. It is more desirable to change airflow velocity by changing blade speed than by changing blade pitch [REF 1]. A direct current motor and controller was recycled from a neighboring wind tunnel to serve this purpose. Unfortunately, the shaft did not align with the fan when the motor was mounted and it required a smaller coupling to accommodate the smaller shaft diameter. The mounting surface consisted of an aluminum plate bolted to the wooden frame of the wind tunnel. The plate was removed and the wooden surface was cut away with a router to allow the mounting plate to be recessed as shown in Figure 15. The motor was then installed and connected to the fan

shaft with a new flexible coupling. The system was started and it was discovered that the flow was in the wrong direction. Research determined that this motor could be operated in either direction so the controller was disassembled and rewired to allow the motor to provide the correct flow.



Figure 15. Recessed Motor Mounting Plate

F. TRAVERSE MECHANISM

The traverse mechanism used in this project was recycled from a neighboring wind tunnel. It was a three axis unit of aluminum construction fabricated by Velmex and shown in Figure 16. In what would become the x-axis in the orientation used in this project, the mechanism was out of alignment. Upon further inspection, it was discovered that the belt driving the twin lead screws was loose. Additionally, the drive nut on one of the slides was loose and slipping. The mechanism was disassembled, cleaned, and lubricated. All of the drive nuts were tightened enough to provide a positive grip on the lead screw without stalling the motors. The belt shown in Figure 17 was tightened and the system was reassembled.

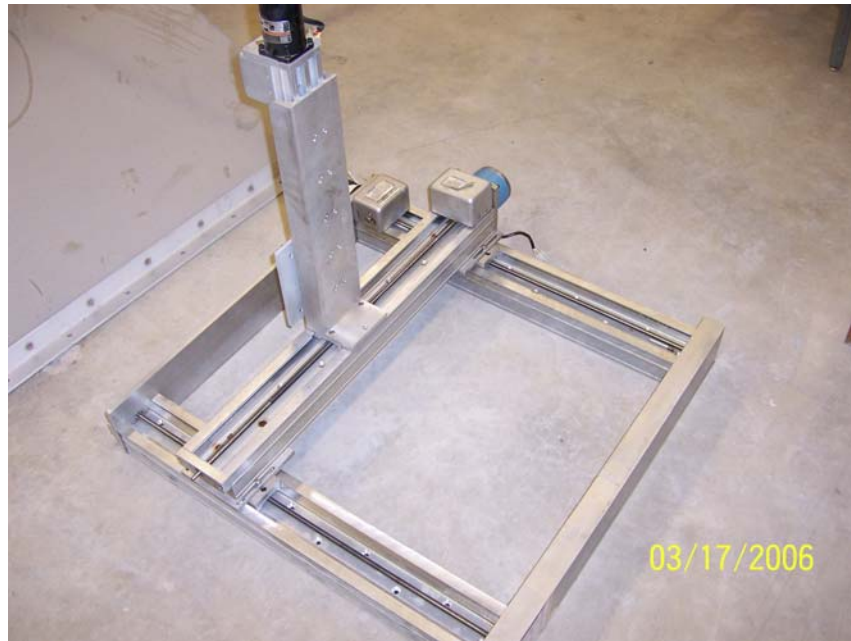


Figure 16. Traverse Mechanism



Figure 17. Traverse Mechanism Drive Belt

Next, a suitable mounting table was obtained. The table surface was raised to an appropriate height for the wind tunnel test section. Aluminum L-brackets were fabricated for locating the mechanism on the table. The table was then bolted to the wind tunnel frame for a positive and stationary location. The mechanism was shimmed to a level position. A bracket was then fabricated for attachment of the anemometer probe holder to the z-axis slider of the traverse mechanism. Then a probe holder was constructed of

carbon fiber reinforced spruce wood and was clamped to the mechanism bracket with a pair of C-clamps. The end of the probe holder was carefully dilled and cut to receive the anemometer probe and thermocouple. A thin plastic screw was utilized to clamp the probes in position at the end of the holder. The holder was shaped in an elliptical cross section to minimize wind disturbance in the flow field.

III. EXPERIMENTAL SETUP

A. WIND TUNNEL

1. Description

The NPS MAV wind tunnel is an open circuit design with the intake and test section mounted horizontally. After the test section, the flow is turned upward through guide vanes and driven by an axial fan powered from an electric motor. The facility has an overall length of 13 feet. It is 84 inches tall at the tip of the stator cone at the exhaust and at the upper intake lip. The entire structure is supported by a wooden frame with casters for mobility. The intake begins with a half section of 10 inch diameter piping along all four sides as a bellmouth, as is used in the University of New Mexico facility [REF 7]. A bellmouth type intake helps reduce losses, but, more importantly in this application, it helps provide a more uniform flow [REF 9]. The settling chamber consists of the honeycomb section along with two layers of screen and their associated settling regions. Honeycomb followed by screen combinations have proven to be the best method of reducing turbulence [REF 12]. This completes the intake and marks the beginning of the contraction. A splitter plate is not used in this facility. The intake and contraction section are illustrated in Figure 18.

The honeycomb section is “a guiding device through which the individual air filaments are rendered parallel” according to Prandtl [REF 11]. The section used in this facility had a cell size of .25 inches and a thickness of 1.375 inches. This yields a length to size ratio of 5.5. Almost complete elimination of the lateral components of turbulence occurs in the range of 5-10 [REF 8]. The section was aluminum in construction. This is superior to impregnated paper honeycombs sometimes used because the aluminum provides more precise dimensions and leads to better flow characteristics [REF 8]. The cell size should be smaller than the smallest lateral wavelength of velocity variation. This means roughly 150 cells per settling chamber ‘diameter’ or 25,000 cells in total for adequate results [REF 8]. The facility has approximately 38,800 cells and the additional number of cells compensates for the slightly smaller than typical length to cell size ratio.

Honeycombs themselves shed small scale turbulence, so the honeycomb should be placed upstream of the screens to minimize the turbulence level, as is done in this tunnel.

Screens in the settling chamber make flow velocity more uniform by imposing a pressure drop proportional to the velocity squared. They also tend to reduce the boundary layer thickness and refract incident flow toward the normal. The most important function in this application is the ability of screens to reduce turbulence intensity. The screens were made of .01 inch diameter wire with a mesh size of .05 inches. The screens should be placed 50-75 mesh diameters apart so that the screen shed turbulence has decayed [REF 12]. The screens in the facility are spaced at 3.25 inches in their mounting frames for a spacing of 65 mesh diameters.

The intake is 45 inches high and 54 inches wide yielding a contraction ratio of 6.75. The main effects of a contraction section are to reduce the mean and fluctuating velocity variations to a smaller fraction of the average and to increase the average mean velocity. Contraction ratios between 6 and 10 have been found to be adequate in small, low speed tunnels [REF 8]. The wall shape of a contraction is based on producing a uniform steady stream at the outlet of the section. This would dictate a long contraction. However, this must be balanced with the desire to minimize the size of the boundary layer, favoring a short contraction. A short contraction section also moves the flow closer to boundary layer separation and flow unsteadiness. Additionally, the concave shape at the contraction inlet has a destabilizing effect on the boundary layer while the convex shape at the exit tends to stabilize the flow. A desirable design would then dictate that separation is just avoided (a minimum length) and the nonuniformity at the exit is tolerable, typically less than 1% variation in mean streamwise velocity outside the boundary layers [REF 8]. From the flow analysis on the tunnel it will be shown that the contraction design is satisfactory. The contraction section is shown in Figure 18.



Figure 18. Intake and Contraction Sections

The length of the contracting section is 40 inches, thus the length to height ratio is .89, within the range of similar wind tunnels and exactly the same as the Mixing Layer Tunnel at NASA Ames [REF 9]. The contraction is three dimensional. The wall contour shape is unknown; however the statistics are similar to the fifth order polynomial contraction used in the boundary layer tunnel at NASA Ames [REF 9]. While the actual form of the contour is not that important, the smoothness in the contour shape is critical. Figure 18 shows that this section is quite smooth. It is also important that the ends be smooth and the second radius of curvature be less than the first, and that the ends join the parallel sections so smoothly that the first and second derivatives of the curvature are close to zero [REF 8] as shown in Figure 19.

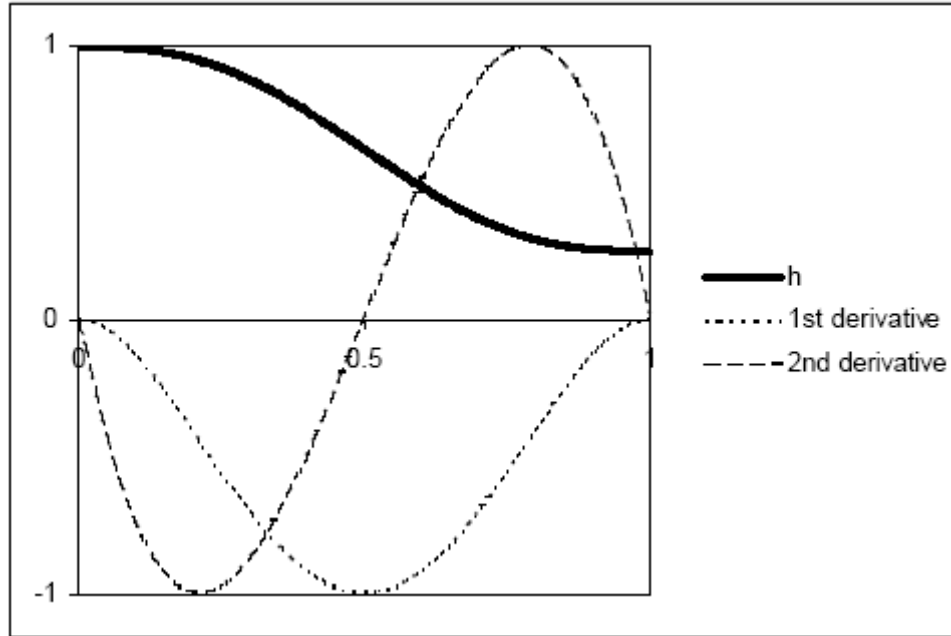


Figure 19. Contraction Contour [From REF 14]

The test section is 53 inches long and made of plexiglass. The test section is rectangular and measures 15 inches high and 24 inches wide. The cross section design is not critical and depends on the needs of the user [REF 8]. The entire ceiling of this section can be raised for access necessary for testing. There are two supports over the test section length for mounting to the frame.

The airflow is driven by an axial fan near the exhaust. While prerotation vanes are normally used, it is acceptable for a lightly loaded fan, as in this application, to use a set of straightener vanes downstream of the fan as long as the number of fan blades is different from the number of straightener vanes [REF 9]. The fan has 4 blades while the stator has 9 blades and a center cone. The fan is turned by a Minarik Electric direct current motor and a Motor Master controller.

B. TRAVERSE MECHANISM

The traverse mechanism was a Velmex Unislide model B4026P40J with a Bodine Electric DC stepping motor type 34T1BEHD attached for motion in the x-direction. The y-direction was controlled by a Velmex Unislide model B4027P40J with a Superior

Electric stepping motor M091-FD09, and the z-axis was regulated by a Velmex Unislide model B2515 P40J with A Bodine Electric DC stepping motor type 23T2BEHD attached. All of the motors were capable of 200 steps per revolution. This allowed for 16,000 counts per inch of movement when combined with the lead screw pitch. The mechanism was controlled by a Velmex VP 9003 controller.

C. CONSTANT TEMPERATURE ANEMOMETER

1. Equipment Used

The constant temperature anemometer (hotwire system) used was a Dantec Streamline 90N10 frame with five 90C10 CTA modules. The data was processed by a Pentium computer running Streamware software version 3.4 after being fed through a National Instruments A/D board model BNC-2090. The hotwire system was calibrated with a dedicated calibration unit, the Dantec Streamline 90H02 flow unit code 9090H0021 serial 149.

2. Theory of Operation

A hotwire flow measurement system consists of the components shown in Figure 20 below. The probe used was a miniature wire unit as this type is recommended for unidirectional gas flows with turbulence intensity up to 10% because they have the highest frequency response. The probe consists of a $5\ \mu\text{m}$ diameter tungsten wire 1 mm long supported by stainless steel prongs at each end. The prongs are then coated in a ceramic with the ends connecting to a probe support and connected to the anemometer through a probe cable.

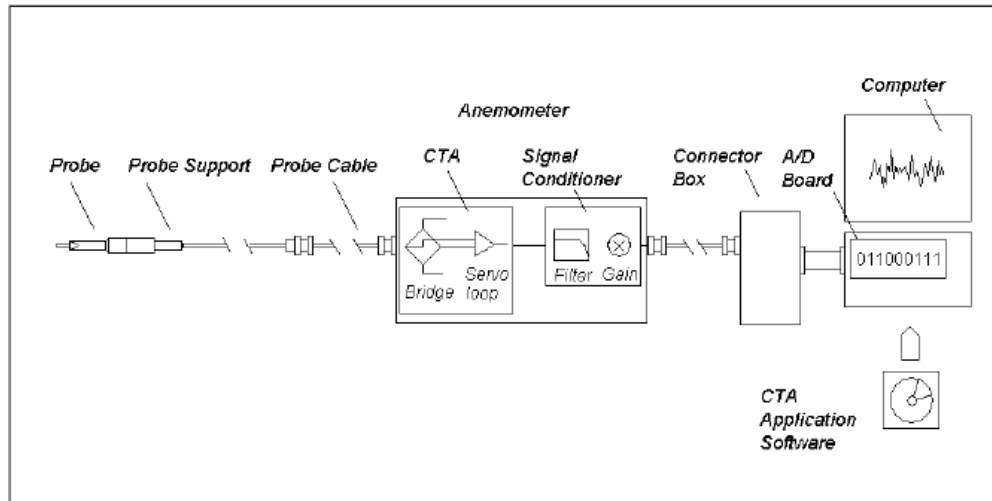


Figure 20. Hotwire Measuring System [from REF 10]

The probe wire's resistance changes with its temperature. This then becomes the measurement leg of a Wheatstone bridge opposite a variable resistor, which defines the operating resistance, and hence the operating temperature of the instrument. The system also contains a thermocouple in the flow field next to the hot wire probe for temperature compensation. When the bridge is in balance, no voltage difference exists across its diagonal. If the flow velocity were to increase, more heat would be transferred away from the wire and its temperature would go down so its resistance would go down resulting in an error voltage at the input of the current regulating amplifier. This will cause the probe current to increase. The wire will heat and increase in resistance until the balance is restored. The current regulating amplifier has a very high gain so a condition of bridge balance exists almost independent of the flow velocity past the wire. The response time of the wire is thus reduced to a few micro seconds. The probe current is calculated by the voltage drop across the bridge. In this way the system calculates flow velocity at very high frequencies based on the heat transfer from the wire.

D. MAV MODEL

The NPS MAV model was constructed by Professor Kevin Jones. It was similar to the flying MAV but without the rudder. The model had a much larger fuselage to house the more robust motor and transmission, while the flying craft places motor,

transmission, battery, and radio gear in a smaller space. This allowed the model to operate indefinitely, while the flying MAV motor has a limited lifetime. Additionally, the main lifting wings in the model shown below are covered with Japanese tissue paper while the operational aircraft used the same microfilm plastic sheeting that covers the flapping wings.

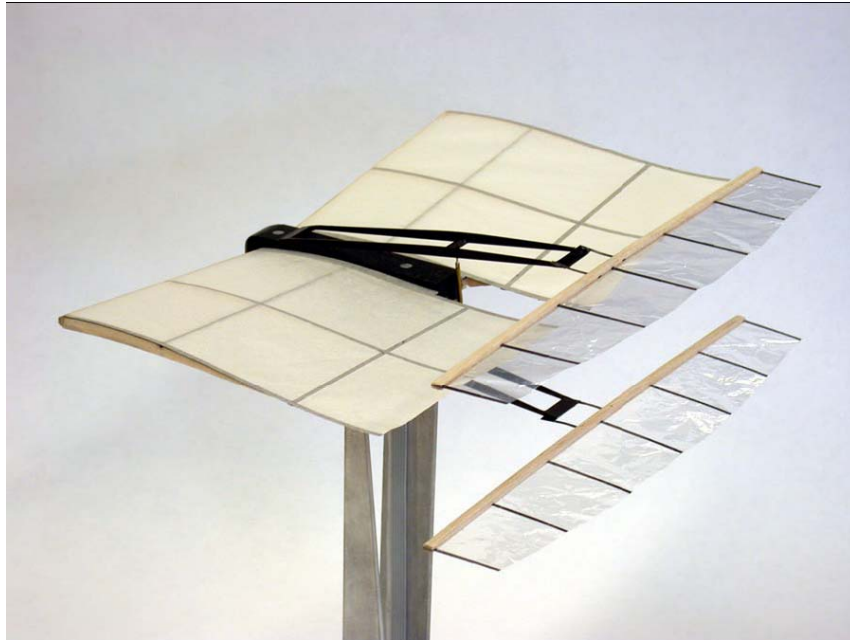


Figure 21. NPS MAV Model [From REF 4]

The frame of the main wing was composed entirely of light weight balsa wood and carbon fiber assembled with a cyanoacrylate adhesive in a sandwich fashion. The main wings were slightly wider than the flapping wings at 10.5 inches with a mean geometric chord of 5.5 inches. The main wings were rectangular in shape and mounted with 8.5 degrees of dihedral.

The flapping wings were powered by a small electric motor run from an external power supply for this project. To power the model, an Elenco model MX-9300 power supply was used. The model flapping frequency was measured using a strobe light. A chart was developed relating motor voltage to flapping frequency and used during the experiment.

The flapping wings were driven from the motor, through the transmission and to a crankshaft. The crankshaft converted the rotation of the motor to linear motion required for the flapping wings by driving connecting rods to each flapping beam. The flapping beams were of carbon fiber sandwich construction common to the other structural members. The flapping beams were attached to the front of the fuselage on one end and the flexible wing mounts on the other. The plunging motion of the flapping wings was caused by the motor's rotation while the pitching motion was aeroelastic. As the flexible wing mounts at the end of the flapping beams flexed, the pitch was induced in the flapping wings. The amount of pitch was related to the stiffness of the flexible wing mounts. The flapping wings functioned in counterphase to eliminate the inertial and aerodynamic effects of a single wing moving up and down. The flapping wings were identical in construction, each having a chord of 1.5 inches in the midspan and tapered at the ends with a span of 9.75 inches. The flapping wings are tapered to limit spanwise oscillations of the wing and provide no noticeable decrease in thrust. The leading edge was constructed of balsawood dowel. The surface was covered with thin plastic film supported at seven points with chordwise ribs of carbon fiber sandwich construction. Two layers of the rib material run two thirds of the chord length and a third layer runs to the trailing edge of the wing. Although multiple crankshafts and connecting rods were available to adjust the plunging amplitude and mean separation, for the experiment, the plunging amplitude, from the centerline to top-dead-center, is 1 inch or 0.67 chord lengths, with a mean separation of 3 inches.

E. PITOT TUBE FLOW REFERENCE

A small pitot tube was used as a reference free stream velocity for different data runs. The tube was connected to a MKS Baratron type 223BD pressure transducer powered by an Analog Devices type 904 power supply. The voltage is read by a Metex ME-11 voltmeter. This system was calibrated by the hotwire and the resulting chart is located in Appendix B.

IV. EXPERIMENTAL PROCEDURE AND RESULTS

A. CALIBRATION

The hotwire system was calibrated using its own calibration module for maximum accuracy. The calibration module operates from a pressurized air supply and creates a free jet. The free jet is produced through a high resolution control valve and a series of Laval nozzles that provide a stable mass flow regardless of back pressure. Thus the free jet velocity is highly accurate and adjustable to fractions of a percent. The probe and thermocouple were attached to the module with the hotwire sensor positioned directly in the flow. The module was set to calibrate from 1 to 10 m/s in accordance with the testing velocities of interest in 10 points arranged logarithmically as recommended by the manufacturer. This resulted in the table in Appendix C with a fourth order polynomial fit according to the equation $U = C_0 + C_1 E_{corr} + C_2 E_{corr}^2 + C_3 E_{corr}^3 + C_4 E_{corr}^4$.

B. FLOW VERIFICATION OF THE TUNNEL

1. The Grid

The grid used in the flow verification of the tunnel consisted of a plane in the x or streamwise, direction. The y direction was taken horizontally with the z direction in the vertical. The origin was taken as the center of the tunnel with the negative y direction running to the left side of the center and the negative z direction extending below the center of the test section. Data was taken at 31 positions in the y direction at 7 different z positions. Boundary layer effects were captured on the left side starting .125 inches from the wall. Ten points were taken within an inch of the wall and the rest of the points were spaced one inch apart across the tunnel. The traverse mechanism did not have sufficient travel to obtain boundary layer information from both sides of the test section. It was assumed to be similar on all sides. No vehicle testing will ever be conducted so close to the wall so the important part of the flow was fully mapped.

2. The Procedure

The probes were aligned with the flow and mounted in the specially fabricated holder and attached to the traverse mechanism as shown in Figure 22. The traverse mechanism was positioned at the required points and data was recorded. The sampling rate was 40 KHz and 10,000 samples were taken. The data were reduced with Dantec Streamware software. The data taken is included in the appendices.



Figure 22. Anemometer Probes

3. Results at 2 m/s

The entire plane was sampled at tunnel speeds of 2, 3, and 5 m/s with the complete results shown in Appendices D, E, and F. Figure 24 shows the turbulence intensity distribution at a free stream velocity of 2 m/s. Turbulence intensity ranges from .575 % to .83 % at this speed with an average of .712 %. No particular pattern or trend is evident in the data.

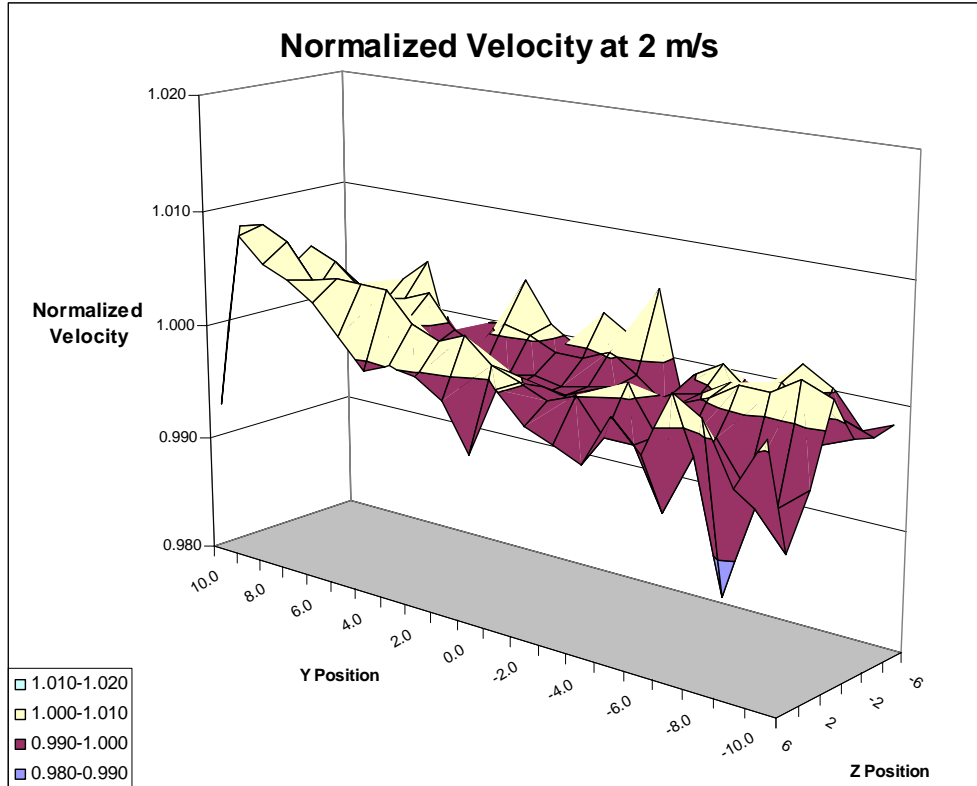


Figure 23. Normalized Velocity at 2 m/s

Another useful performance measure is the variation in velocity across the test section. In a perfect flow there would be no variation and no turbulence. Values of velocity variation across good quality wind tunnel test sections are often quoted in the .2-.3% range [REF 1]. The velocity variation for this facility was computed by calculating the percent difference between the velocity at a point and the mean velocity. The absolute value was then taken and these values averaged. At 2 m/s the average velocity variation was .251 %, well within quoted values for quality wind tunnels. Figure 23 shows the normalized velocity distribution. Considering the scale of the axis, the data appear to be evenly scattered with extreme values near the top, bottom, and sides of the test section.

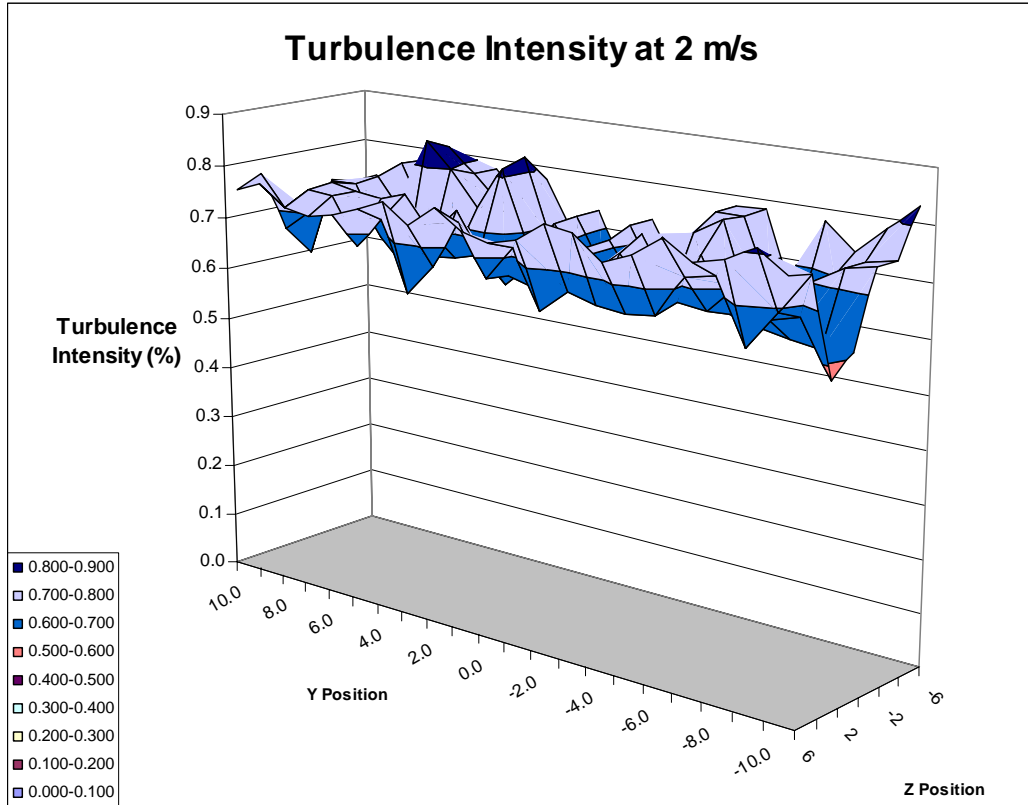


Figure 24. Turbulence Intensity at 2 m/s

4. Results at 3 m/s

At a tunnel velocity of 3 m/s, the turbulence intensity decreased to an average of .569% with the distribution shown in Figure 26. This downward trend in turbulence with an increase in velocity has been shown in past experiments. The normalized velocity distribution is shown in Figure 25 while the average variation at this speed was .165%.

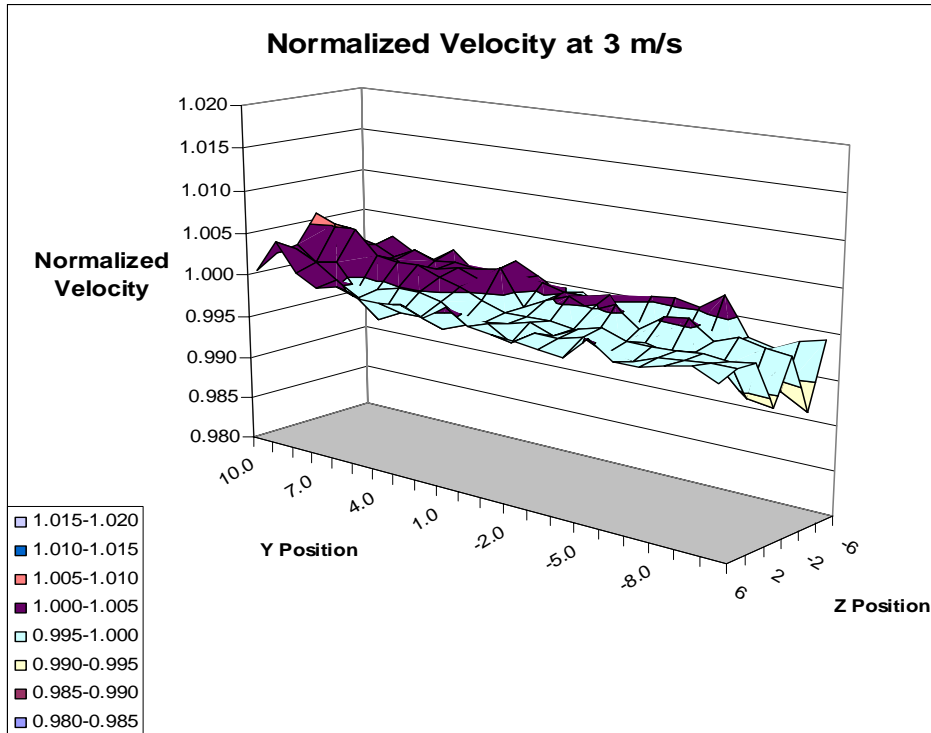


Figure 25. Normalized Velocity at 3 m/s

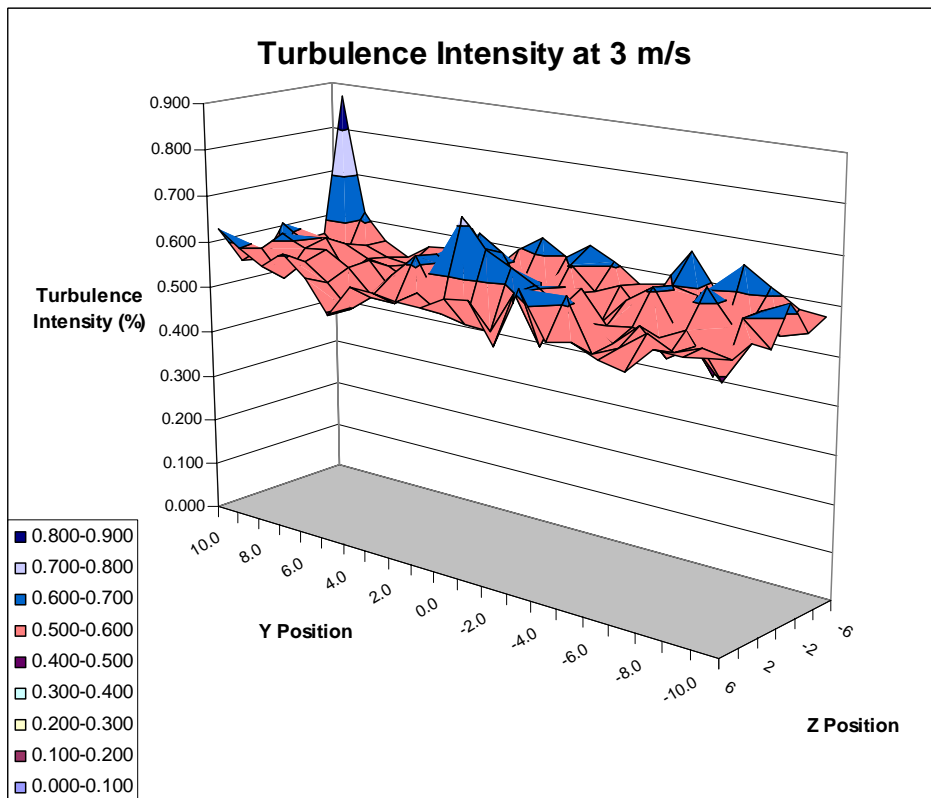


Figure 26. Turbulence Intensity at 3 m/s

5. Results at 5 m/s

At 5 m/s the turbulence intensity crept lower to .511% and is shown in Figure 28.

Figure 27 shows the normalized velocities with an average variation of .125%.

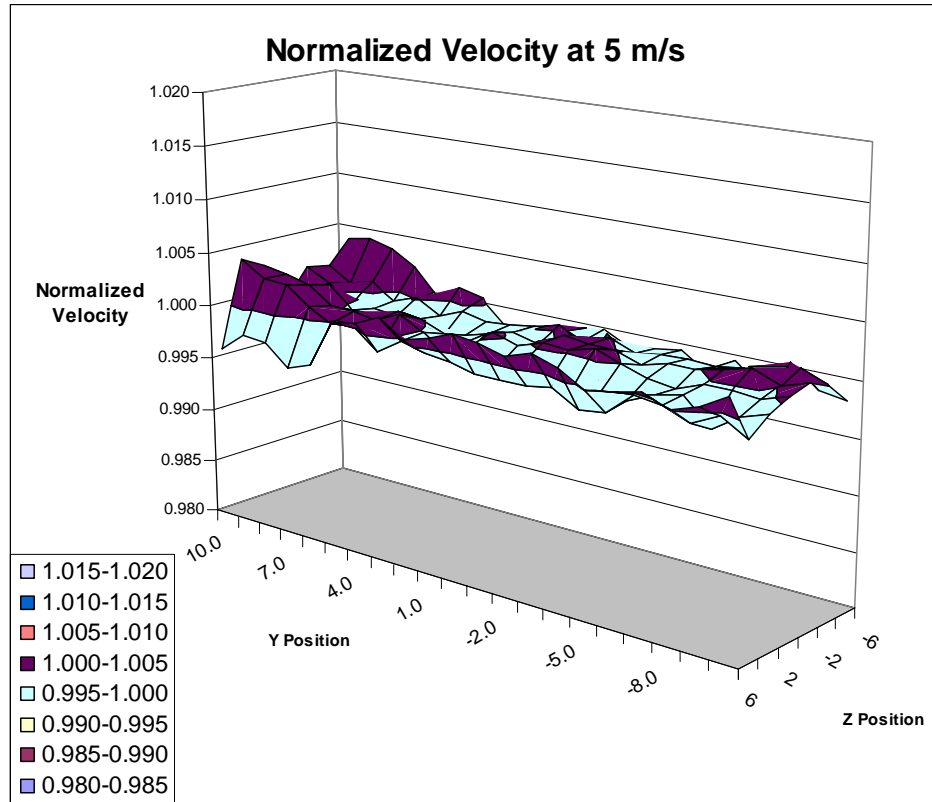


Figure 27. Normalized Velocity at 5 m/s

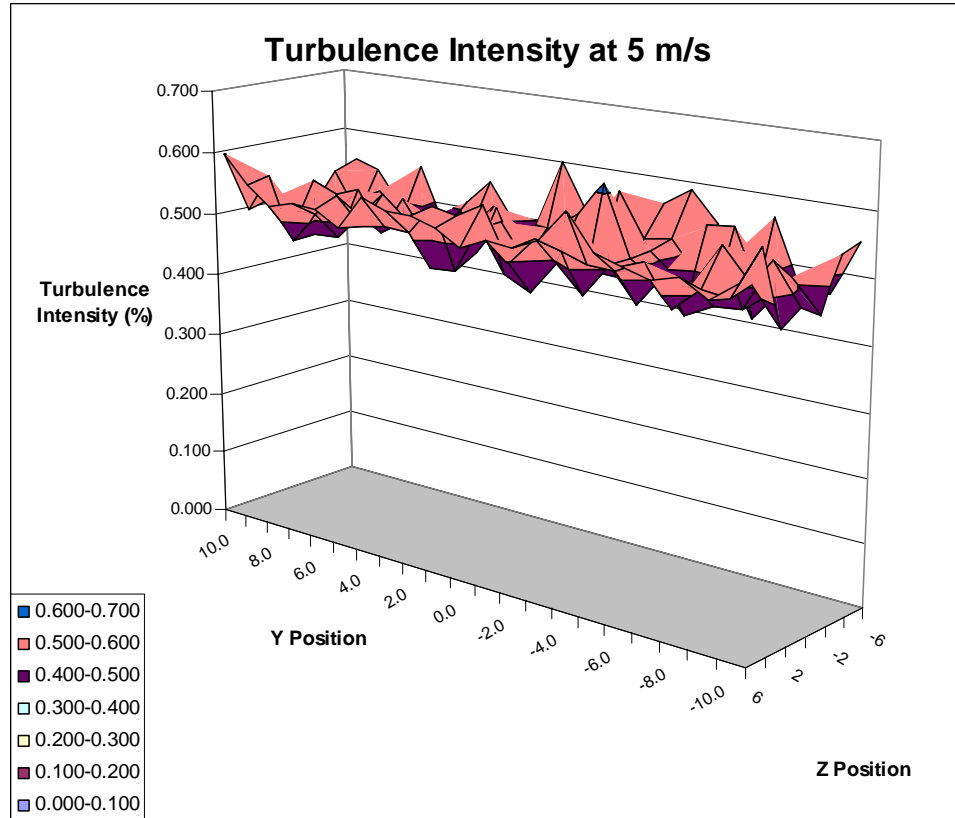


Figure 28. Turbulence Intensity at 5 m/s

C. MODEL WAKE

1. Flapping Wing Wake

With a reasonable flow established in the wind tunnel, the next step was to analyze the MAV model wake in the facility. Initially, the model was mounted vertically without the main wing to see the unaltered wake of the flapping wings as shown in Figure 29. All of the wakes shown were measured with the hotwire and are thus time averaged.

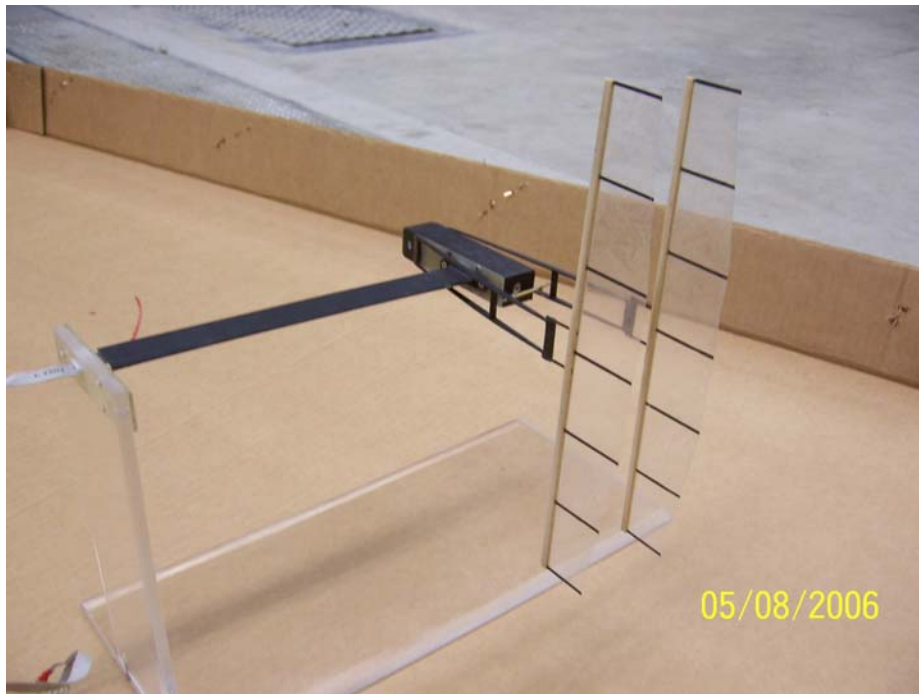


Figure 29. Vertical Model Without Main Wing

The model was run at 20 Hz and 30 Hz for comparison. The hotwire was then traversed horizontally across the wake 10 inches on either side of the model near the centerline. The normalized velocity profile is shown in Figure 30 with a polynomial curve fit in bold. The curves are quite symmetric; especially when the polynomial fit is considered. This graphic clearly shows the effect of the individual wings. The velocity deficit between the wings at 3 m/s may indicate that the MAV must flap at a higher frequency to travel at 3 m/s. Alternatively, the mean separation could be lengthened to eliminate the deficit. Figure 31 shows the wake when flapping at 30 Hz, still indicating a slight velocity deficit in the center at 3 m/s. The wake appears to be somewhat narrower when operating at lower frequencies. Overall, the peak velocities are higher when flapping at 30 Hz. This illustrates the conclusion that flapping faster creates more thrust. In fact, thrust should increase with the square of frequency, according to the linear theory of waves and instabilities.

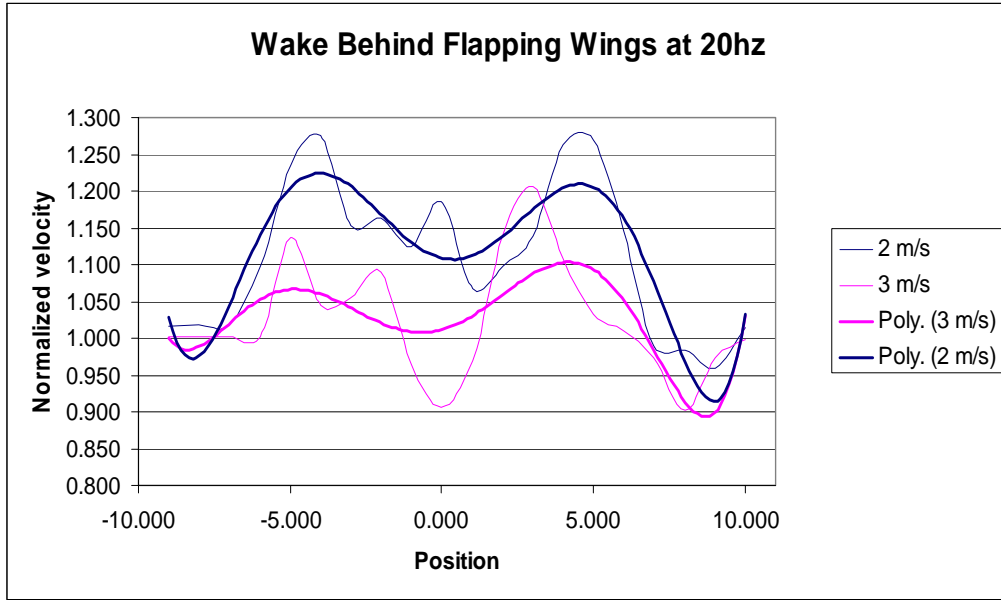


Figure 30. Flapping Wing Wake at 20 Hz

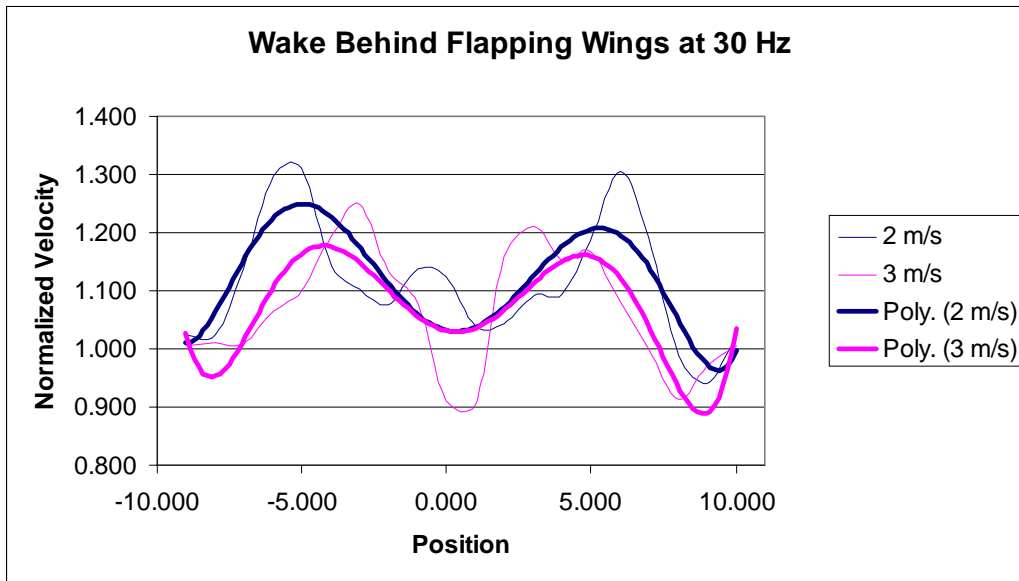


Figure 31. Flapping Wing Wake at 30 Hz

2. Wake Behind Complete Model

Next, the main wings were added. The model remained mounted vertically as shown in Figure 32. The wake was measured at a plane 19 inches from the leading edge of the upper flapping wing. This shifted the wake to the left side of the tunnel (positive y

values) in accordance with the 15° angle of attack (AOA) as shown in Figure 33. This AOA is typical in flight and the model was mounted in this way for a more accurate representation of flight. Figure 34 shows the wake shift when flapping at 30 Hz, again near the centerline of the model. The 3 m/s velocity deficit appears to grow when flapping faster.

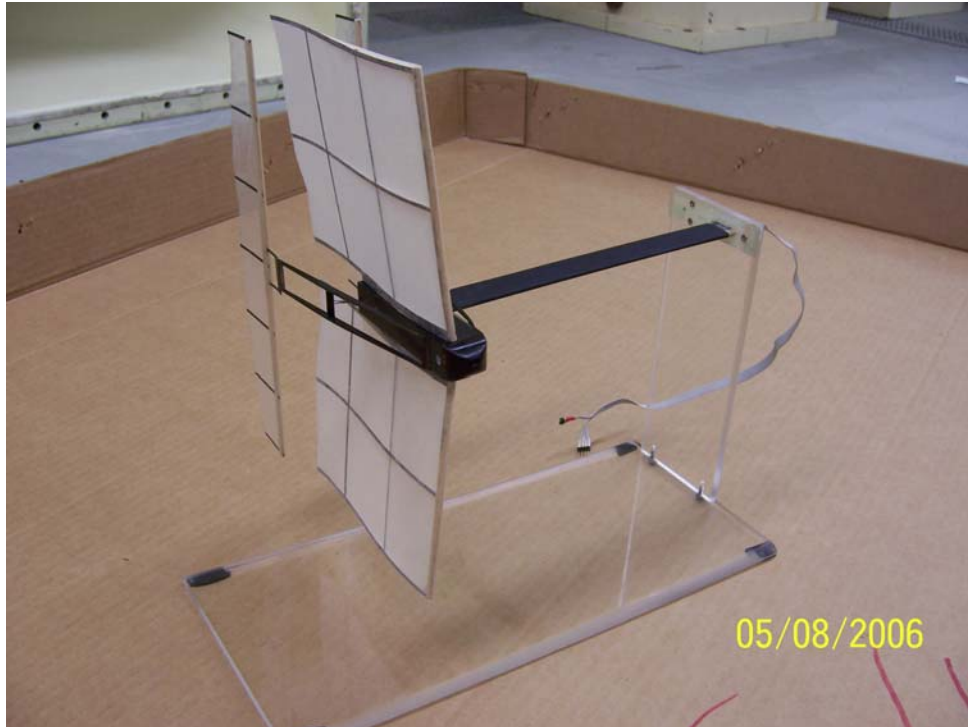


Figure 32. Vertical Model With Main Wings

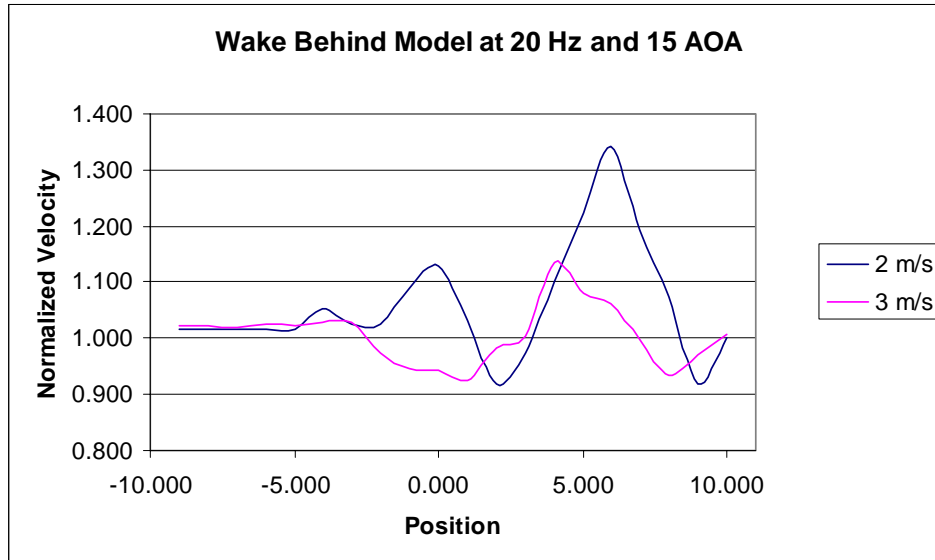


Figure 33. Wake Behind Complete Model at 20 Hz

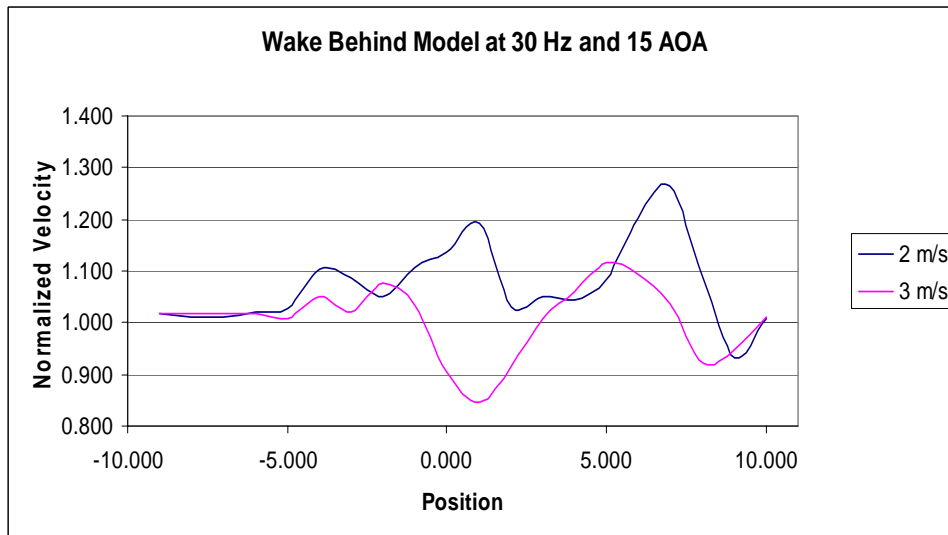


Figure 34. Wake Behind Complete Model at 30 Hz



Figure 35. Complete Horizontal Model in the Test Section

3. Full Wake Characterization

Finally, the model was mounted horizontally and the complete plane of the wake was analyzed. The MAV was run at 30 Hz with freestream velocities of 2 m/s and 3 m/s and the wake was analyzed 19 inches downstream of the leading edge of the flapping wings. The wake was sampled in elevation from -5 to 5 inches in 1 inch increments. Each elevation was sampled in 31 points along the y axis, from -7.5 to 7.5 in .5 inch increments. The results from the 2 m/s run are displayed in Figure 36, with the 3 m/s data in Figure 37. While the flapping wings are 9.75 inches across, the wake assumes a different shape. At freestream velocity of 2 m/s, the bulk of the wake is concentrated in an area 3-5 inches wide but nearly the entire height of the test section. A similar trend is seen at 3 m/s with less intensity. While the flapping wings have a mean separation of 3 inches, the wake has some level of intensity 10 inches in height. The wake appears to shift from short and wide coming off of the flapping wings to tall and thin a short distance downstream. Figure 38 illustrates the vortex structure of the wake. Considerable entrainment of the flow begins to occur around the leading edge of the flapping wings. At flight frequencies, the vortices do not change sign although they fluctuate in strength [REF15]. The top view of figure 38 was seen in flow visualization

in figure 42. The wake is drawn centerline, bringing the y axis size of the wake down. The aft and side views of figure 38 show the vortex structure driving the wake larger in the z direction as seen by the hotwire measurements.

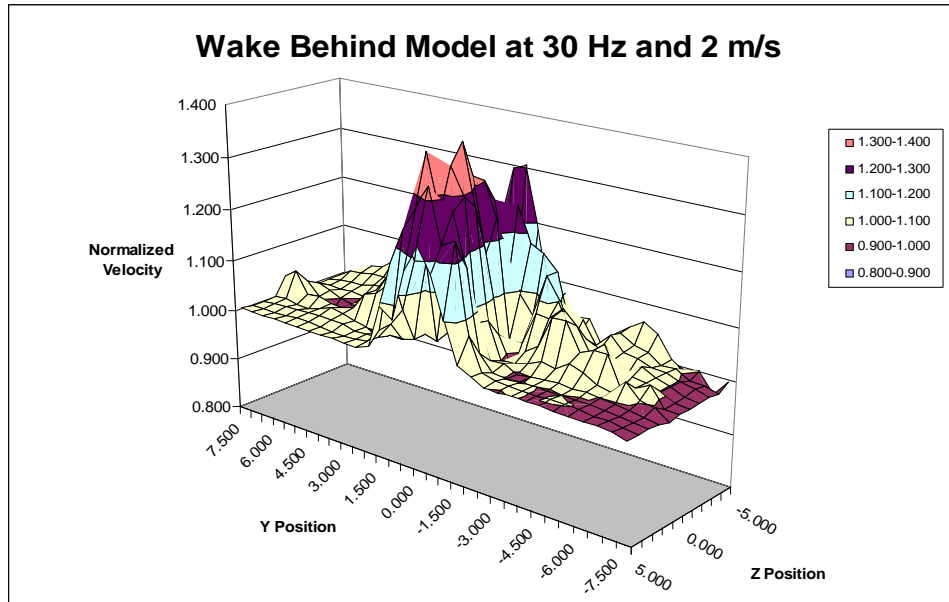


Figure 36. Model Wake at 2 m/s

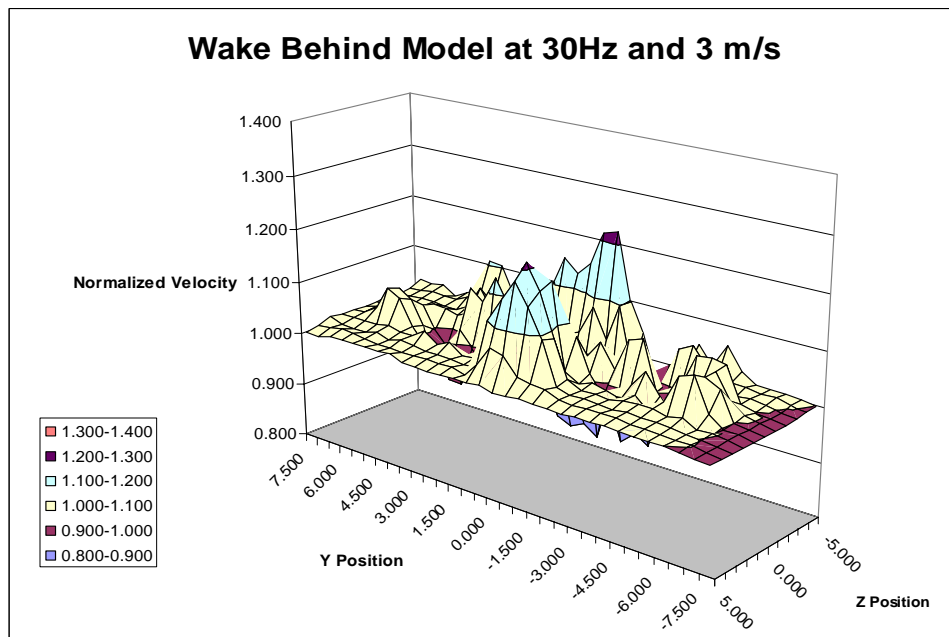


Figure 37. Model Wake at 3 m/s

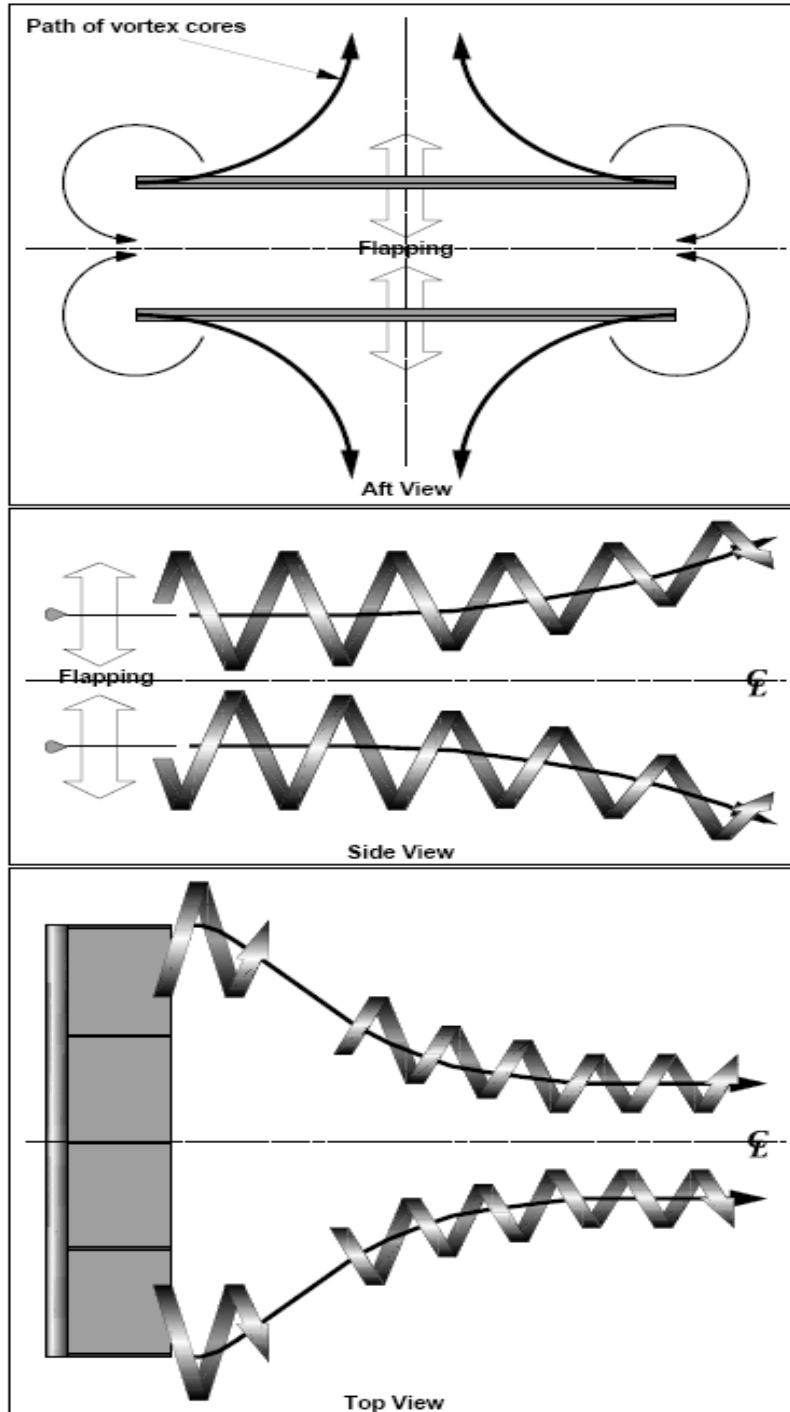


Figure 38. Sketch of Vortex Structures [From REF 15]

D. FLOW VISUALIZATION

To further investigate the flow around the model, flow visualization techniques were used with a smoke wire. A .075 mm tungsten wire was obtained and knots of copper wire were wrapped around it and soldered in place at 1 cm intervals. The ends were crimped in a piece of brass tubing and inserted through a special fitting. The fitting surrounded the wire and fed Roscoe fog fluid around the wire. The wire was strung vertically in the tunnel and heated with a variac. The fluid was dripped over the wire and pooled around the copper knots. As the wire heated, the fluid would produce smoke that would flow through the tunnel as streaklines. These lines lasted for several seconds. Experimentation revealed the voltage setting, amount of fluid on the wire, and tunnel speed all to be critical to successful flow visualization. The best variac setting appeared to be about 12 volts, and the best lines were produced after allowing the wire to cool briefly before starting the variac. The tunnel was operated at 2 m/s and the model was placed in the test section in various orientations and positions. The action was captured by a 3 CCD Sony digital video recorder model number DCR VX-1000.

Figure 39 shows the main wing in stall with the model stationary. The stall region is large and encompasses the entire upper flapping wing. Not only is this a major problem concerning lift, the flapping wing would not be effective in this stalled flow. Figure 40 shows the model operating. The flow is reattached by the entrainment that occurs from the flapping motion. Lift and propulsion are restored.

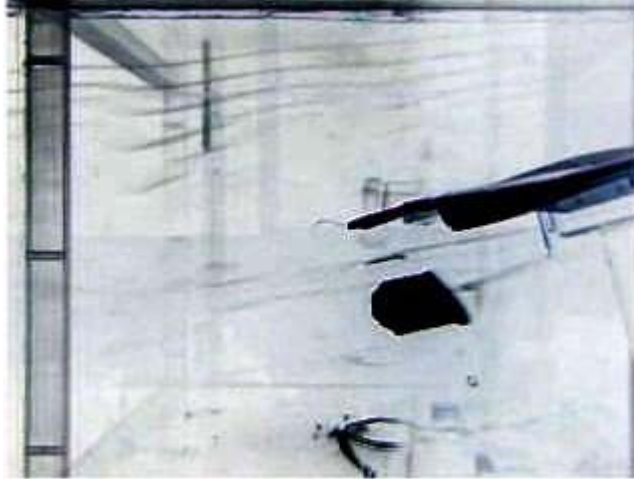


Figure 39. Main Wing Stalled When Not Flapping

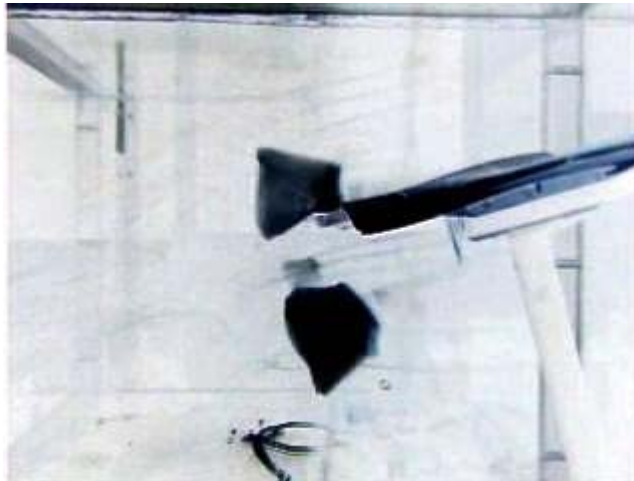


Figure 40. Flow Reattaches When Flapping

The wingtip vortex is illustrated in Figure 41 below. Low aspect ratio wings, like the ones on the NPS MAV, have demonstrated an ability to resist stall. This is because wing tip vortices reattach the flow along the outer surfaces, restoring a significant amount of lift.

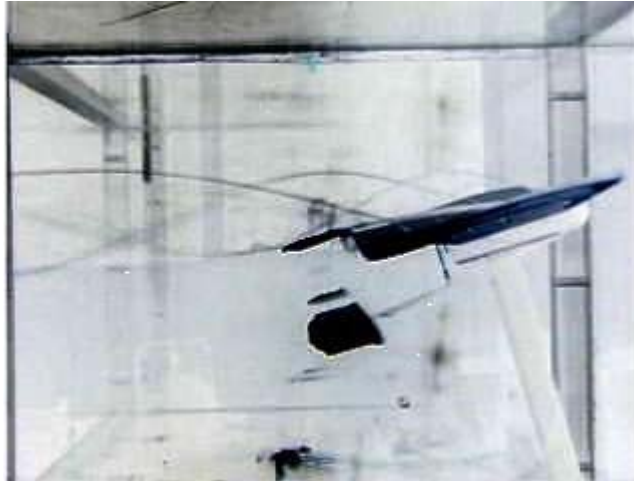


Figure 41. Wingtip Vortex

As shown in Figures 36 and 37, the MAV wake is more intense toward the centerline of the craft. In the flow visualization below, the streaklines clearly move in this direction, creating the higher intensity wake in the vertical plane. This is also seen in the top view of the vortex structure of figure 38.



Figure 42. Wake Drawn Toward Centerline

THIS PAGE INTENTIONALLY LEFT BLANK

V. CONCLUSIONS

A. TUNNEL FLOW VERIFICATION

Ideally, a wind tunnel would produce a flow outside the boundary layer such that the velocity passing through each plane normal to the centerline would be uniformly parallel to the centerline and would have no variation with time [REF 1]. While this goal is not achievable in reality, real facilities need to generate flow of sufficient quality to fulfill their intended purpose. Values for velocity variation across the test section of high quality wind tunnels are often quoted in the .2-.3% range. This gives a dynamic pressure variation of .4 -.6% [REF 1]. The NPS MAV wind tunnel velocity variation ranged from .125% at 5 m/s to .251% at 2 m/s. This appears to be satisfactory for MAV testing.

B. MODEL WAKE

The model wake shifts to a vertical orientation some distance behind it. This information was supported by flow visualization.

The wingtip vortices were shown reattaching the flow to the main wings at the outer surfaces. This supports the MAVs ability to fly at low speeds with significant angles of attack.

The action of the flapping wings acts to entrain the flow and reattach it to the main wings. The MAV is virtually stall proof in flight.

C. RECOMMENDATIONS FOR FURTHER IMPROVEMENT

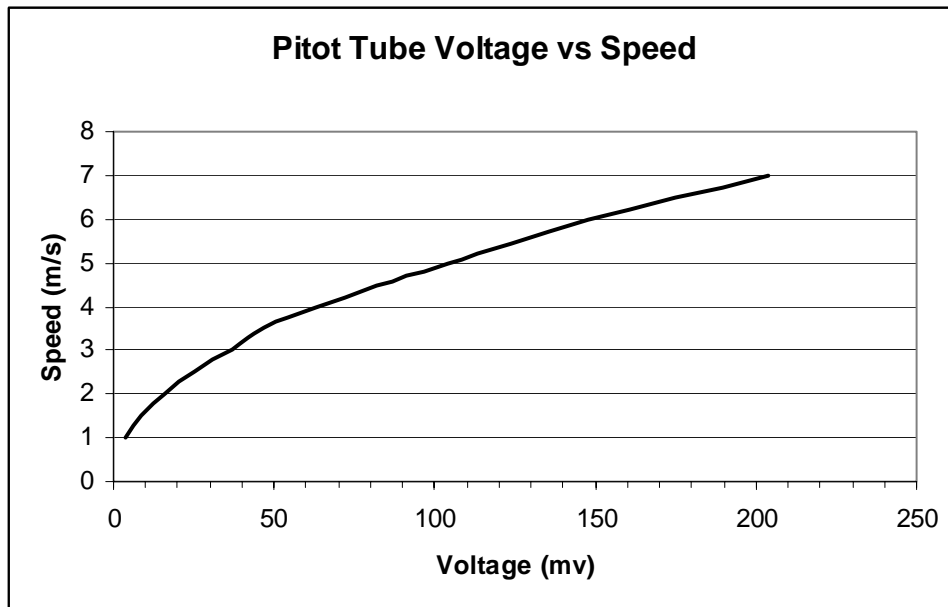
Further improvements could be seen in the flow by extending the intake and adding more layers of screen. Some low turbulence tunnels have as many as eleven screen sections. In order to accomplish this addition the intake would have to be removed. The same mounting design could be utilized with additional hardware. The

frame section that supports the intake would have to be lengthened and a larger support fabricated to fit under the longer intake section.

As vibration is a possible source of measurement error, the tunnel vibration could be reduced by remounting the motor and fan with dampers. This would limit the vibration transferred to the frame. Additionally, the test section exit could be replaced with a rubber unit that would limit the structural vibration.

APPENDIX A. PITOT TUBE CALIBRATION

Voltage (mv)	voltage change (mv)	Tunnel speed (m/s)	speed (ft/s)	speed (mph)
3.7	3.7	1	3.28	2.24
8.5	4.8	1.5	4.92	3.36
16	7.5	2	6.56	4.47
25	9	2.5	8.20	5.59
37	12	3	9.84	6.71
47	10	3.5	11.48	7.83
63	16	4	13.12	8.95
82	19	4.5	14.76	10.07
104	22	5	16.40	11.18
148	44	6	19.69	13.42
204	56	7	22.97	15.66



THIS PAGE INTENTIONALLY LEFT BLANK

APPENDIX B. HOTWIRE CALIBRATION

U1	E1	T	P (kpa)	E1 corr	U1 calc		Fourth order polynomial	
m/s	volts	C		volts	m/s			
1.017	1.904	23.033	101.347	1.908	1.016		c0	1.977103
1.317	1.971	23.035	101.347	1.975	1.32		c1	-8.082218
1.677	2.039	23.041	101.344	2.043	1.677		c2	9.588953
2.171	2.117	23.046	101.341	2.121	2.168		c3	-5.088278
2.818	2.203	23.048	101.347	2.208	2.818		c4	1.123862
3.616	2.291	23.053	101.352	2.296	3.617			
4.685	2.388	23.057	101.358	2.393	4.678			
6.061	2.494	23.071	101.344	2.499	6.087			
7.653	2.59	23.072	101.347	2.595	7.628			
9.942	2.709	23.074	101.347	2.715	9.95			

THIS PAGE INTENTIONALLY LEFT BLANK

APPENDIX C. FLOW VERIFICATION AT 2 M/S

z = 6.0						z = 4.0					
z	y	U mean	U/U ∞	T%	U var %	z	y	U mean	U/U ∞	T%	U var %
6.0	11.875	1.224	0.597	1.316	40.313	4.0	11.875	1.163	0.567	1.411	43.298
6.0	11.813	1.511	0.737	1.125	26.318	4.0	11.813	1.554	0.758	1.161	24.235
6.0	11.750	1.771	0.864	0.960	13.639	4.0	11.750	1.754	0.855	1.027	14.484
6.0	11.688	2.044	0.997	0.864	0.327	4.0	11.688	1.942	0.947	0.865	5.318
6.0	11.625	2.039	0.994	0.854	0.570	4.0	11.625	2.065	1.007	0.819	0.678
6.0	11.500	2.047	0.998	0.825	0.180	4.0	11.500	2.064	1.006	0.835	0.630
6.0	11.375	2.053	1.001	0.781	0.112	4.0	11.375	2.072	1.010	0.866	1.020
6.0	11.250	2.057	1.003	0.765	0.307	4.0	11.250	2.071	1.010	0.770	0.971
6.0	11.125	2.054	1.002	0.779	0.161	4.0	11.125	2.066	1.007	0.682	0.727
6.0	11.000	2.044	0.997	0.811	0.327	4.0	11.000	2.063	1.006	0.741	0.581
6.0	10.000	2.037	0.993	0.757	0.668	4.0	10.000	2.064	1.006	0.779	0.630
6.0	9.000	2.068	1.008	0.778	0.844	4.0	9.000	2.065	1.007	0.722	0.678
6.0	8.000	2.064	1.006	0.738	0.649	4.0	8.000	2.063	1.006	0.763	0.581
6.0	7.000	2.062	1.006	0.730	0.551	4.0	7.000	2.057	1.003	0.761	0.288
6.0	6.000	2.059	1.004	0.741	0.405	4.0	6.000	2.058	1.003	0.672	0.337
6.0	5.000	2.054	1.002	0.761	0.161	4.0	5.000	2.058	1.003	0.731	0.337
6.0	4.000	2.049	0.999	0.784	0.083	4.0	4.000	2.058	1.003	0.601	0.337
6.0	3.000	2.051	1.000	0.746	0.015	4.0	3.000	2.053	1.001	0.660	0.093
6.0	2.000	2.050	1.000	0.789	0.034	4.0	2.000	2.051	1.000	0.752	0.004
6.0	1.000	2.047	0.998	0.753	0.180	4.0	1.000	2.053	1.001	0.656	0.093
6.0	0.000	2.039	0.994	0.741	0.570	4.0	0.000	2.049	0.999	0.721	0.102
6.0	-1.000	2.051	1.000	0.755	0.015	4.0	-1.000	2.047	0.998	0.615	0.199
6.0	-2.000	2.046	0.998	0.793	0.229	4.0	-2.000	2.045	0.997	0.661	0.297
6.0	-3.000	2.044	0.997	0.785	0.327	4.0	-3.000	2.047	0.998	0.646	0.199
6.0	-4.000	2.042	0.996	0.742	0.424	4.0	-4.000	2.041	0.995	0.641	0.492
6.0	-5.000	2.051	1.000	0.763	0.015	4.0	-5.000	2.041	0.995	0.648	0.492
6.0	-6.000	2.046	0.998	0.802	0.229	4.0	-6.000	2.031	0.990	0.725	0.979
6.0	-7.000	2.057	1.003	0.769	0.307	4.0	-7.000	2.031	0.990	0.736	0.979
6.0	-8.000	2.054	1.002	0.784	0.161	4.0	-8.000	2.040	0.995	0.620	0.541
6.0	-9.000	2.044	0.997	0.811	0.327	4.0	-9.000	2.045	0.997	0.691	0.297
6.0	-10.000	2.053	1.001	0.774	0.112	4.0	-10.000	2.049	0.999	0.765	0.102
	U ∞ =	2.051		AVG	0.301		U ∞ =	2.051		AVG	0.393

		U				U					
z	y	mean	U/U ∞	T%	U var %	z	y	mean	U/U ∞	T%	U var %
2.0	11.875	1.202	0.585	1.248	41.530	0.0	11.875	1.194	0.579	1.111	42.051
2.0	11.813	1.405	0.683	1.022	31.655	0.0	11.813	1.486	0.721	1.013	27.879
2.0	11.750	1.703	0.828	0.914	17.159	0.0	11.750	1.720	0.835	0.816	16.522
2.0	11.688	1.807	0.879	0.823	12.100	0.0	11.688	1.937	0.940	0.760	5.991
2.0	11.625	2.032	0.988	0.690	1.155	0.0	11.625	2.012	0.976	0.828	2.351
2.0	11.500	2.069	1.006	0.734	0.645	0.0	11.500	2.054	0.997	0.674	0.312
2.0	11.375	2.071	1.007	0.680	0.742	0.0	11.375	2.069	1.004	0.729	0.416
2.0	11.250	2.067	1.005	0.682	0.548	0.0	11.250	2.067	1.003	0.743	0.319
2.0	11.125	2.069	1.006	0.744	0.645	0.0	11.125	2.068	1.004	0.746	0.367
2.0	11.000	2.068	1.006	0.773	0.596	0.0	11.000	2.067	1.003	0.748	0.319
2.0	10.000	2.066	1.005	0.661	0.499	0.0	10.000	2.068	1.004	0.603	0.367
2.0	9.000	2.064	1.004	0.704	0.402	0.0	9.000	2.064	1.002	0.756	0.173
2.0	8.000	2.064	1.004	0.769	0.402	0.0	8.000	2.060	1.000	0.756	0.021
2.0	7.000	2.060	1.002	0.759	0.207	0.0	7.000	2.060	1.000	0.661	0.021
2.0	6.000	2.059	1.002	0.754	0.159	0.0	6.000	2.062	1.001	0.612	0.076
2.0	5.000	2.057	1.001	0.770	0.061	0.0	5.000	2.058	0.999	0.641	0.118
2.0	4.000	2.055	1.000	0.703	0.036	0.0	4.000	2.056	0.998	0.645	0.215
2.0	3.000	2.058	1.001	0.755	0.110	0.0	3.000	2.053	0.996	0.662	0.361
2.0	2.000	2.055	1.000	0.677	0.036	0.0	2.000	2.059	0.999	0.613	0.070
2.0	1.000	2.052	0.998	0.651	0.182	0.0	1.000	2.055	0.997	0.661	0.264
2.0	0.000	2.055	1.000	0.635	0.036	0.0	0.000	2.055	0.997	0.652	0.264
2.0	-1.000	2.054	0.999	0.660	0.085	0.0	-1.000	2.056	0.998	0.711	0.215
2.0	-2.000	2.053	0.999	0.684	0.133	0.0	-2.000	2.058	0.999	0.621	0.118
2.0	-3.000	2.054	0.999	0.727	0.085	0.0	-3.000	2.053	0.996	0.752	0.361
2.0	-4.000	2.058	1.001	0.666	0.110	0.0	-4.000	2.058	0.999	0.655	0.118
2.0	-5.000	2.050	0.997	0.660	0.279	0.0	-5.000	2.059	0.999	0.732	0.070
2.0	-6.000	2.050	0.997	0.653	0.279	0.0	-6.000	2.061	1.000	0.635	0.027
2.0	-7.000	2.052	0.998	0.707	0.182	0.0	-7.000	2.064	1.002	0.622	0.173
2.0	-8.000	2.045	0.995	0.657	0.522	0.0	-8.000	2.064	1.002	0.611	0.173
2.0	-9.000	2.043	0.994	0.673	0.620	0.0	-9.000	2.067	1.003	0.603	0.319
2.0	-10.000	2.041	0.993	0.575	0.717	0.0	-10.000	2.065	1.002	0.610	0.222
	U ∞ =	2.056		AVG	0.261		U ∞ =	2.060		AVG	0.185

		U						U			
z	y	mean	U/U ∞	T%	U var %	z	y	mean	U/U ∞	T%	U var %
-2.0	11.875	1.106	0.539	1.019	46.052	-4.0	11.875	1.114	0.543	1.019	45.667
-2.0	11.813	1.456	0.710	0.926	28.980	-4.0	11.813	1.423	0.694	0.926	30.596
-2.0	11.750	1.735	0.846	0.839	15.371	-4.0	11.750	1.745	0.851	0.839	14.891
-2.0	11.688	1.897	0.925	0.761	7.469	-4.0	11.688	1.891	0.922	0.740	7.770
-2.0	11.625	2.001	0.976	0.706	2.396	-4.0	11.625	2.013	0.982	0.695	1.819
-2.0	11.500	2.062	1.006	0.680	0.579	-4.0	11.500	2.054	1.002	0.682	0.180
-2.0	11.375	2.064	1.007	0.741	0.677	-4.0	11.375	2.039	0.994	0.736	0.551
-2.0	11.250	2.061	1.005	0.704	0.530	-4.0	11.250	2.045	0.997	0.733	0.259
-2.0	11.125	2.066	1.008	0.710	0.774	-4.0	11.125	2.041	0.995	0.735	0.454
-2.0	11.000	2.062	1.006	0.855	0.579	-4.0	11.000	2.061	1.005	0.873	0.522
-2.0	10.000	2.061	1.005	0.740	0.530	-4.0	10.000	2.057	1.003	0.729	0.327
-2.0	9.000	2.059	1.004	0.700	0.433	-4.0	9.000	2.054	1.002	0.682	0.180
-2.0	8.000	2.055	1.002	0.762	0.238	-4.0	8.000	2.051	1.000	0.780	0.034
-2.0	7.000	2.054	1.002	0.695	0.189	-4.0	7.000	2.053	1.001	0.682	0.131
-2.0	6.000	2.051	1.000	0.848	0.042	-4.0	6.000	2.055	1.002	0.827	0.229
-2.0	5.000	2.047	0.998	0.800	0.153	-4.0	5.000	2.049	0.999	0.781	0.064
-2.0	4.000	2.046	0.998	0.734	0.201	-4.0	4.000	2.047	0.998	0.733	0.161
-2.0	3.000	2.045	0.997	0.815	0.250	-4.0	3.000	2.052	1.001	0.828	0.083
-2.0	2.000	2.045	0.997	0.668	0.250	-4.0	2.000	2.051	1.000	0.683	0.034
-2.0	1.000	2.046	0.998	0.726	0.201	-4.0	1.000	2.049	0.999	0.732	0.064
-2.0	0.000	2.045	0.997	0.653	0.250	-4.0	0.000	2.049	0.999	0.634	0.064
-2.0	-1.000	2.046	0.998	0.713	0.201	-4.0	-1.000	2.051	1.000	0.731	0.034
-2.0	-2.000	2.047	0.998	0.637	0.153	-4.0	-2.000	2.048	0.999	0.635	0.112
-2.0	-3.000	2.044	0.997	0.701	0.299	-4.0	-3.000	2.044	0.997	0.685	0.307
-2.0	-4.000	2.048	0.999	0.752	0.104	-4.0	-4.000	2.050	1.000	0.780	0.015
-2.0	-5.000	2.049	0.999	0.786	0.055	-4.0	-5.000	2.053	1.001	0.779	0.131
-2.0	-6.000	2.052	1.001	0.633	0.091	-4.0	-6.000	2.049	0.999	0.634	0.064
-2.0	-7.000	2.047	0.998	0.651	0.153	-4.0	-7.000	2.052	1.001	0.649	0.083
-2.0	-8.000	2.046	0.998	0.701	0.201	-4.0	-8.000	2.047	0.998	0.701	0.161
-2.0	-9.000	2.045	0.997	0.734	0.250	-4.0	-9.000	2.048	0.999	0.735	0.112
-2.0	-10.000	2.047	0.998	0.746	0.153	-4.0	-10.000	2.046	0.998	0.746	0.210
	U ∞ =	2.050		AVG	0.226		U ∞ =	2.050		AVG	0.142

z	y	U mean	U/U ∞	T%	U var %
-6.0	11.875	1.122	0.547	0.980	45.283
-6.0	11.813	1.512	0.737	0.860	26.264
-6.0	11.750	1.743	0.850	0.861	14.999
-6.0	11.688	1.929	0.941	0.726	5.928
-6.0	11.625	2.010	0.980	0.697	1.978
-6.0	11.500	2.052	1.001	0.634	0.070
-6.0	11.375	2.061	1.005	0.728	0.509
-6.0	11.250	2.042	0.996	0.735	0.418
-6.0	11.125	2.056	1.003	0.681	0.265
-6.0	11.000	2.058	1.004	0.715	0.363
-6.0	10.000	2.047	0.998	0.733	0.174
-6.0	9.000	2.049	0.999	0.683	0.076
-6.0	8.000	2.055	1.002	0.779	0.216
-6.0	7.000	2.059	1.004	0.680	0.411
-6.0	6.000	2.044	0.997	0.732	0.320
-6.0	5.000	2.043	0.996	0.783	0.369
-6.0	4.000	2.051	1.000	0.731	0.021
-6.0	3.000	2.059	1.004	0.777	0.411
-6.0	2.000	2.052	1.001	0.682	0.070
-6.0	1.000	2.049	0.999	0.732	0.076
-6.0	0.000	2.056	1.003	0.632	0.265
-6.0	-1.000	2.053	1.001	0.731	0.119
-6.0	-2.000	2.062	1.006	0.630	0.558
-6.0	-3.000	2.041	0.995	0.735	0.466
-6.0	-4.000	2.045	0.997	0.782	0.271
-6.0	-5.000	2.040	0.995	0.784	0.515
-6.0	-6.000	2.047	0.998	0.635	0.174
-6.0	-7.000	2.054	1.002	0.779	0.168
-6.0	-8.000	2.051	1.000	0.731	0.021
-6.0	-9.000	2.045	0.997	0.782	0.271
-6.0	-10.000	2.047	0.998	0.830	0.174
	U ∞ =	2.051		AVG	0.250

Overall velocity variation at 2 m/s (%) 0.251

Average turbulence intensity at 2 m/s (%) 0.712

APPENDIX D. FLOW VERIFICATION AT 3 M/S

z = 6.0						z = 4.0					
z	y	U mean	U/U ∞	T%	U var %	z	y	U mean	U/U ∞	T%	U var %
6.0	11.875	2.579	0.833	11.035	16.742	4.0	11.875	2.720	0.878	10.026	12.164
6.0	11.813	2.789	0.900	8.528	9.963	4.0	11.813	2.947	0.952	5.544	4.834
6.0	11.750	2.930	0.946	5.938	5.411	4.0	11.750	3.102	1.002	1.297	0.172
6.0	11.688	2.997	0.968	4.424	3.248	4.0	11.688	3.071	0.992	3.761	0.829
6.0	11.625	2.986	0.964	5.411	3.603	4.0	11.625	3.109	1.004	0.907	0.398
6.0	11.500	3.078	0.994	2.358	0.633	4.0	11.500	3.111	1.005	0.782	0.462
6.0	11.375	3.089	0.997	1.932	0.278	4.0	11.375	3.109	1.004	0.903	0.398
6.0	11.250	3.105	1.002	1.416	0.239	4.0	11.250	3.111	1.005	0.701	0.462
6.0	11.125	3.104	1.002	1.194	0.207	4.0	11.125	3.114	1.006	0.658	0.559
6.0	11.000	3.108	1.003	1.082	0.336	4.0	11.000	3.110	1.004	0.560	0.430
6.0	10.000	3.100	1.001	0.634	0.077	4.0	10.000	3.104	1.002	0.552	0.236
6.0	9.000	3.112	1.005	0.600	0.465	4.0	9.000	3.107	1.003	0.589	0.333
6.0	8.000	3.102	1.001	0.571	0.142	4.0	8.000	3.103	1.002	0.532	0.204
6.0	7.000	3.098	1.000	0.607	0.013	4.0	7.000	3.098	1.000	0.579	0.043
6.0	6.000	3.100	1.001	0.563	0.077	4.0	6.000	3.093	0.999	0.543	0.119
6.0	5.000	3.097	1.000	0.496	0.019	4.0	5.000	3.087	0.997	0.495	0.313
6.0	4.000	3.097	1.000	0.564	0.019	4.0	4.000	3.091	0.998	0.530	0.183
6.0	3.000	3.098	1.000	0.562	0.013	4.0	3.000	3.091	0.998	0.528	0.183
6.0	2.000	3.095	0.999	0.556	0.084	4.0	2.000	3.088	0.997	0.562	0.280
6.0	1.000	3.100	1.001	0.551	0.077	4.0	1.000	3.091	0.998	0.528	0.183
6.0	0.000	3.095	0.999	0.581	0.084	4.0	0.000	3.093	0.999	0.518	0.119
6.0	-1.000	3.094	0.999	0.587	0.116	4.0	-1.000	3.088	0.997	0.511	0.280
6.0	-2.000	3.093	0.999	0.506	0.149	4.0	-2.000	3.093	0.999	0.600	0.119
6.0	-3.000	3.092	0.998	0.632	0.181	4.0	-3.000	3.093	0.999	0.505	0.119
6.0	-4.000	3.091	0.998	0.536	0.213	4.0	-4.000	3.095	0.999	0.615	0.054
6.0	-5.000	3.099	1.000	0.549	0.045	4.0	-5.000	3.091	0.998	0.512	0.183
6.0	-6.000	3.093	0.999	0.523	0.149	4.0	-6.000	3.090	0.998	0.535	0.216
6.0	-7.000	3.093	0.999	0.513	0.149	4.0	-7.000	3.093	0.999	0.573	0.119
6.0	-8.000	3.095	0.999	0.566	0.084	4.0	-8.000	3.094	0.999	0.547	0.087
6.0	-9.000	3.097	1.000	0.564	0.019	4.0	-9.000	3.095	0.999	0.568	0.054
6.0	-10.000	3.093	0.999	0.573	0.149	4.0	-10.000	3.095	0.999	0.556	0.054
	U ∞ =	3.098		AVG	0.121		U ∞ =	3.097		AVG	0.178

U						U					
z	y	mean	U/U ∞	T%	U var %	z	y	mean	U/U ∞	T%	U var %
2.0	11.875	2.625	0.848	7.403	15.222	0.0	11.875	2.460	0.797	13.109	20.307
2.0	11.813	2.775	0.896	9.977	10.377	0.0	11.813	2.574	0.834	9.389	16.614
2.0	11.750	2.971	0.960	5.151	4.047	0.0	11.750	2.800	0.907	6.041	9.292
2.0	11.688	3.090	0.998	0.798	0.204	0.0	11.688	2.772	0.898	6.862	10.199
2.0	11.625	3.094	0.999	1.149	0.075	0.0	11.625	2.913	0.944	6.001	5.632
2.0	11.500	3.069	0.991	2.537	0.882	0.0	11.500	2.961	0.959	5.507	4.077
2.0	11.375	3.108	1.004	0.613	0.377	0.0	11.375	3.070	0.995	2.117	0.546
2.0	11.250	3.109	1.004	0.724	0.410	0.0	11.250	3.088	1.000	2.152	0.038
2.0	11.125	3.107	1.003	0.639	0.345	0.0	11.125	3.110	1.008	0.800	0.750
2.0	11.000	3.103	1.002	0.707	0.216	0.0	11.000	3.107	1.007	0.642	0.653
2.0	10.000	3.105	1.003	0.544	0.280	0.0	10.000	3.106	1.006	0.614	0.621
2.0	9.000	3.100	1.001	0.611	0.119	0.0	9.000	3.103	1.005	0.585	0.524
2.0	8.000	3.101	1.002	0.587	0.151	0.0	8.000	3.102	1.005	0.599	0.491
2.0	7.000	3.092	0.999	0.594	0.140	0.0	7.000	3.094	1.002	0.529	0.232
2.0	6.000	3.094	0.999	0.565	0.075	0.0	6.000	3.093	1.002	0.570	0.200
2.0	5.000	3.096	1.000	0.515	0.010	0.0	5.000	3.093	1.002	0.513	0.200
2.0	4.000	3.096	1.000	0.568	0.010	0.0	4.000	3.090	1.001	0.542	0.102
2.0	3.000	3.094	0.999	0.618	0.075	0.0	3.000	3.088	1.000	0.611	0.038
2.0	2.000	3.089	0.998	0.533	0.236	0.0	2.000	3.085	0.999	0.581	0.060
2.0	1.000	3.090	0.998	0.716	0.204	0.0	1.000	3.082	0.998	0.641	0.157
2.0	0.000	3.091	0.998	0.660	0.172	0.0	0.000	3.082	0.998	0.557	0.157
2.0	-1.000	3.093	0.999	0.630	0.107	0.0	-1.000	3.082	0.998	0.579	0.157
2.0	-2.000	3.090	0.998	0.605	0.204	0.0	-2.000	3.081	0.998	0.585	0.189
2.0	-3.000	3.094	0.999	0.568	0.075	0.0	-3.000	3.081	0.998	0.597	0.189
2.0	-4.000	3.096	1.000	0.550	0.010	0.0	-4.000	3.078	0.997	0.531	0.286
2.0	-5.000	3.093	0.999	0.520	0.107	0.0	-5.000	3.081	0.998	0.539	0.189
2.0	-6.000	3.093	0.999	0.566	0.107	0.0	-6.000	3.079	0.997	0.527	0.254
2.0	-7.000	3.093	0.999	0.512	0.107	0.0	-7.000	3.081	0.998	0.553	0.189
2.0	-8.000	3.094	0.999	0.545	0.075	0.0	-8.000	3.078	0.997	0.475	0.286
2.0	-9.000	3.093	0.999	0.489	0.107	0.0	-9.000	3.069	0.994	0.599	0.578
2.0	-10.000	3.094	0.999	0.575	0.075	0.0	-10.000	3.068	0.994	0.549	0.610
	U ∞ =	3.096		AVG	0.121		U ∞ =	3.087		AVG	0.289

U						U					
z	y	mean	U/U ∞	T%	U var %	z	y	mean	U/U ∞	T%	U var %
-2.0	11.875	2.341	0.753	12.631	24.652	-4.0	11.875	2.658	0.855	9.322	14.474
-2.0	11.813	2.606	0.839	7.396	16.123	-4.0	11.813	2.641	0.850	7.983	15.021
-2.0	11.750	2.674	0.861	8.497	13.934	-4.0	11.750	2.772	0.892	6.502	10.806
-2.0	11.688	2.796	0.900	6.360	10.007	-4.0	11.688	2.966	0.954	4.936	4.564
-2.0	11.625	2.797	0.900	5.505	9.975	-4.0	11.625	3.024	0.973	3.703	2.698
-2.0	11.500	2.972	0.957	4.361	4.343	-4.0	11.500	3.105	0.999	1.831	0.091
-2.0	11.375	3.066	0.987	2.302	1.317	-4.0	11.375	3.115	1.002	1.396	0.230
-2.0	11.250	3.110	1.001	1.096	0.099	-4.0	11.250	3.130	1.007	0.823	0.713
-2.0	11.125	3.118	1.004	0.848	0.357	-4.0	11.125	3.121	1.004	0.563	0.423
-2.0	11.000	3.115	1.003	0.791	0.260	-4.0	11.000	3.120	1.004	0.601	0.391
-2.0	10.000	3.112	1.002	0.566	0.164	-4.0	10.000	3.115	1.002	0.572	0.230
-2.0	9.000	3.114	1.002	0.580	0.228	-4.0	9.000	3.113	1.002	0.526	0.166
-2.0	8.000	3.108	1.000	0.576	0.035	-4.0	8.000	3.110	1.001	0.561	0.070
-2.0	7.000	3.111	1.001	0.553	0.131	-4.0	7.000	3.114	1.002	0.544	0.198
-2.0	6.000	3.106	1.000	0.544	0.030	-4.0	6.000	3.111	1.001	0.536	0.102
-2.0	5.000	3.110	1.001	0.519	0.099	-4.0	5.000	3.112	1.001	0.532	0.134
-2.0	4.000	3.112	1.002	0.548	0.164	-4.0	4.000	3.111	1.001	0.582	0.102
-2.0	3.000	3.109	1.001	0.556	0.067	-4.0	3.000	3.112	1.001	0.548	0.134
-2.0	2.000	3.115	1.003	0.653	0.260	-4.0	2.000	3.110	1.001	0.508	0.070
-2.0	1.000	3.102	0.998	0.622	0.158	-4.0	1.000	3.110	1.001	0.550	0.070
-2.0	0.000	3.106	1.000	0.533	0.030	-4.0	0.000	3.108	1.000	0.533	0.005
-2.0	-1.000	3.109	1.001	0.540	0.067	-4.0	-1.000	3.108	1.000	0.604	0.005
-2.0	-2.000	3.106	1.000	0.566	0.030	-4.0	-2.000	3.110	1.001	0.556	0.070
-2.0	-3.000	3.109	1.001	0.515	0.067	-4.0	-3.000	3.097	0.997	0.579	0.349
-2.0	-4.000	3.102	0.998	0.569	0.158	-4.0	-4.000	3.099	0.997	0.521	0.284
-2.0	-5.000	3.108	1.000	0.609	0.035	-4.0	-5.000	3.098	0.997	0.600	0.317
-2.0	-6.000	3.109	1.001	0.523	0.067	-4.0	-6.000	3.099	0.997	0.589	0.284
-2.0	-7.000	3.103	0.999	0.629	0.126	-4.0	-7.000	3.102	0.998	0.532	0.188
-2.0	-8.000	3.106	1.000	0.557	0.030	-4.0	-8.000	3.100	0.997	0.558	0.252
-2.0	-9.000	3.104	0.999	0.600	0.094	-4.0	-9.000	3.088	0.994	0.537	0.638
-2.0	-10.000	3.103	0.999	0.627	0.126	-4.0	-10.000	3.083	0.992	0.554	0.799
	U ∞ =	3.107		AVG	0.110		U ∞ =	3.108		AVG	0.221

z	y	U mean	U/U ∞	T%	U var %
-6.0	11.875	2.284	0.746	9.466	25.418
-6.0	11.813	2.317	0.757	10.734	24.340
-6.0	11.750	2.413	0.788	9.987	21.205
-6.0	11.688	2.463	0.804	8.254	19.572
-6.0	11.625	2.618	0.855	7.596	14.511
-6.0	11.500	2.704	0.883	6.997	11.703
-6.0	11.375	2.819	0.921	5.770	7.947
-6.0	11.250	2.893	0.945	5.859	5.531
-6.0	11.125	2.852	0.931	6.649	6.870
-6.0	11.000	2.969	0.970	4.363	3.049
-6.0	10.000	3.064	1.001	0.875	0.053
-6.0	9.000	3.069	1.002	0.618	0.216
-6.0	8.000	3.065	1.001	0.559	0.086
-6.0	7.000	3.063	1.000	0.532	0.020
-6.0	6.000	3.068	1.002	0.565	0.183
-6.0	5.000	3.062	1.000	0.572	0.012
-6.0	4.000	3.063	1.000	0.622	0.020
-6.0	3.000	3.068	1.002	0.546	0.183
-6.0	2.000	3.064	1.001	0.596	0.053
-6.0	1.000	3.059	0.999	0.631	0.110
-6.0	0.000	3.061	1.000	0.599	0.045
-6.0	-1.000	3.056	0.998	0.634	0.208
-6.0	-2.000	3.059	0.999	0.608	0.110
-6.0	-3.000	3.064	1.001	0.570	0.053
-6.0	-4.000	3.065	1.001	0.581	0.086
-6.0	-5.000	3.063	1.000	0.659	0.020
-6.0	-6.000	3.069	1.002	0.580	0.216
-6.0	-7.000	3.056	0.998	0.648	0.208
-6.0	-8.000	3.054	0.997	0.614	0.274
-6.0	-9.000	3.058	0.999	0.579	0.143
-6.0	-10.000	3.060	0.999	0.574	0.078
	U ∞ =	3.062		AVG	0.113

Overall velocity variation at 3 m/s (%) 0.165

Average turbulence intensity at 3 m/s (%) 0.569

APPENDIX E. FLOW VERIFICATION AT 5 M/S

z = 6.0						z = 4.0					
z	y	U mean	U/U ∞	T%	U var %	z	y	U mean	U/U ∞	T%	U var %
6.0	11.875	4.367	0.857	7.984	14.314	4.0	11.875	4.562	0.892	6.457	10.792
6.0	11.813	4.526	0.888	6.801	11.194	4.0	11.813	4.647	0.909	5.801	9.130
6.0	11.750	4.745	0.931	5.482	6.897	4.0	11.750	4.815	0.942	4.757	5.844
6.0	11.688	4.795	0.941	4.906	5.916	4.0	11.688	4.940	0.966	4.187	3.400
6.0	11.625	4.931	0.968	4.597	3.247	4.0	11.625	5.024	0.982	3.422	1.757
6.0	11.500	5.050	0.991	2.465	0.912	4.0	11.500	5.130	1.003	1.007	0.315
6.0	11.375	5.084	0.998	1.368	0.245	4.0	11.375	5.128	1.003	0.880	0.276
6.0	11.250	5.081	0.997	1.061	0.304	4.0	11.250	5.125	1.002	0.714	0.218
6.0	11.125	5.081	0.997	1.969	0.304	4.0	11.125	5.134	1.004	0.603	0.394
6.0	11.000	5.096	1.000	0.976	0.010	4.0	11.000	5.139	1.005	0.561	0.491
6.0	10.000	5.077	0.996	0.601	0.383	4.0	10.000	5.135	1.004	0.502	0.413
6.0	9.000	5.086	0.998	0.558	0.206	4.0	9.000	5.128	1.003	0.564	0.276
6.0	8.000	5.085	0.998	0.530	0.226	4.0	8.000	5.127	1.003	0.466	0.257
6.0	7.000	5.075	0.996	0.542	0.422	4.0	7.000	5.119	1.001	0.515	0.100
6.0	6.000	5.079	0.997	0.538	0.343	4.0	6.000	5.113	1.000	0.551	0.017
6.0	5.000	5.102	1.001	0.517	0.108	4.0	5.000	5.114	1.000	0.510	0.002
6.0	4.000	5.104	1.001	0.571	0.147	4.0	4.000	5.105	0.998	0.518	0.174
6.0	3.000	5.109	1.002	0.557	0.245	4.0	3.000	5.112	1.000	0.514	0.037
6.0	2.000	5.101	1.001	0.556	0.088	4.0	2.000	5.109	0.999	0.563	0.095
6.0	1.000	5.104	1.001	0.543	0.147	4.0	1.000	5.108	0.999	0.554	0.115
6.0	0.000	5.109	1.002	0.521	0.245	4.0	0.000	5.105	0.998	0.578	0.174
6.0	-1.000	5.107	1.002	0.539	0.206	4.0	-1.000	5.105	0.998	0.496	0.174
6.0	-2.000	5.104	1.001	0.536	0.147	4.0	-2.000	5.105	0.998	0.540	0.174
6.0	-3.000	5.108	1.002	0.554	0.226	4.0	-3.000	5.107	0.999	0.529	0.134
6.0	-4.000	5.104	1.001	0.604	0.147	4.0	-4.000	5.100	0.997	0.516	0.271
6.0	-5.000	5.097	1.000	0.552	0.010	4.0	-5.000	5.101	0.997	0.515	0.252
6.0	-6.000	5.099	1.000	0.538	0.049	4.0	-6.000	5.112	1.000	0.536	0.037
6.0	-7.000	5.102	1.001	0.526	0.108	4.0	-7.000	5.110	0.999	0.475	0.076
6.0	-8.000	5.097	1.000	0.538	0.010	4.0	-8.000	5.105	0.998	0.511	0.174
6.0	-9.000	5.101	1.001	0.515	0.088	4.0	-9.000	5.111	0.999	0.508	0.056
6.0	-10.000	5.108	1.002	0.545	0.226	4.0	-10.000	5.104	0.998	0.587	0.193
	U ∞ =	5.097		AVG	0.172		U ∞ =	5.114		AVG	0.168

z	y	U			U var	z	y	U			U var
		mean	U/U ∞	T%	%			mean	U/U ∞	T%	%
2.0	11.875	4.340	0.846	8.801	15.407	0.0	11.875	4.294	0.832	8.802	16.848
2.0	11.813	4.533	0.884	6.658	11.645	0.0	11.813	4.565	0.884	7.019	11.600
2.0	11.750	4.719	0.920	5.766	8.020	0.0	11.750	4.594	0.890	6.536	11.039
2.0	11.688	4.903	0.956	5.213	4.433	0.0	11.688	4.841	0.937	4.842	6.256
2.0	11.625	4.992	0.973	3.206	2.699	0.0	11.625	4.855	0.940	5.334	5.984
2.0	11.500	5.111	0.996	1.827	0.379	0.0	11.500	5.065	0.981	2.656	1.918
2.0	11.375	5.146	1.003	0.940	0.303	0.0	11.375	5.149	0.997	1.059	0.291
2.0	11.250	5.145	1.003	0.703	0.283	0.0	11.250	5.159	0.999	0.672	0.098
2.0	11.125	5.146	1.003	0.568	0.303	0.0	11.125	5.169	1.001	0.675	0.096
2.0	11.000	5.148	1.003	0.514	0.342	0.0	11.000	5.172	1.002	0.557	0.154
2.0	10.000	5.146	1.003	0.514	0.303	0.0	10.000	5.161	0.999	0.471	0.059
2.0	9.000	5.144	1.003	0.475	0.264	0.0	9.000	5.167	1.001	0.542	0.057
2.0	8.000	5.141	1.002	0.468	0.205	0.0	8.000	5.172	1.002	0.525	0.154
2.0	7.000	5.133	1.000	0.470	0.050	0.0	7.000	5.162	1.000	0.539	0.040
2.0	6.000	5.133	1.000	0.513	0.050	0.0	6.000	5.162	1.000	0.476	0.040
2.0	5.000	5.131	1.000	0.554	0.011	0.0	5.000	5.166	1.000	0.500	0.038
2.0	4.000	5.136	1.001	0.520	0.108	0.0	4.000	5.165	1.000	0.529	0.019
2.0	3.000	5.130	1.000	0.451	0.009	0.0	3.000	5.160	0.999	0.491	0.078
2.0	2.000	5.122	0.998	0.453	0.165	0.0	2.000	5.159	0.999	0.473	0.098
2.0	1.000	5.129	1.000	0.527	0.028	0.0	1.000	5.166	1.000	0.528	0.038
2.0	0.000	5.121	0.998	0.463	0.184	0.0	0.000	5.162	1.000	0.475	0.040
2.0	-1.000	5.126	0.999	0.442	0.087	0.0	-1.000	5.166	1.000	0.533	0.038
2.0	-2.000	5.119	0.998	0.496	0.223	0.0	-2.000	5.165	1.000	0.562	0.019
2.0	-3.000	5.120	0.998	0.454	0.204	0.0	-3.000	5.168	1.001	0.615	0.077
2.0	-4.000	5.120	0.998	0.507	0.204	0.0	-4.000	5.164	1.000	0.507	0.001
2.0	-5.000	5.120	0.998	0.456	0.204	0.0	-5.000	5.160	0.999	0.483	0.078
2.0	-6.000	5.125	0.999	0.509	0.106	0.0	-6.000	5.158	0.999	0.438	0.117
2.0	-7.000	5.128	1.000	0.503	0.048	0.0	-7.000	5.163	1.000	0.461	0.020
2.0	-8.000	5.116	0.997	0.567	0.282	0.0	-8.000	5.163	1.000	0.463	0.020
2.0	-9.000	5.124	0.999	0.518	0.126	0.0	-9.000	5.162	1.000	0.543	0.040
2.0	-10.000	5.128	1.000	0.462	0.048	0.0	-10.000	5.166	1.000	0.483	0.038
	U ∞ =	5.130		AVG	0.148		U ∞ =	5.164		AVG	0.057

z = -2.0						z = -4.0					
z	y	U		T%	U var %	z	y	U		T%	U var %
		mean	U/U ∞					mean	U/U ∞		
-2.0	11.875	4.182	0.811	8.625	18.853	-4.0	11.875	4.093	0.792	8.130	20.775
-2.0	11.813	4.284	0.831	7.406	16.874	-4.0	11.813	4.359	0.844	8.658	15.626
-2.0	11.750	4.684	0.909	6.042	9.113	-4.0	11.750	4.541	0.879	6.125	12.103
-2.0	11.688	4.830	0.937	5.217	6.280	-4.0	11.688	4.674	0.905	6.350	9.529
-2.0	11.625	4.876	0.946	4.511	5.387	-4.0	11.625	4.807	0.930	5.738	6.955
-2.0	11.500	5.121	0.994	1.907	0.633	-4.0	11.500	5.014	0.971	3.575	2.948
-2.0	11.375	5.153	1.000	1.066	0.012	-4.0	11.375	5.158	0.998	1.557	0.160
-2.0	11.250	5.167	1.003	0.634	0.260	-4.0	11.250	5.173	1.001	0.878	0.130
-2.0	11.125	5.158	1.001	0.626	0.085	-4.0	11.125	5.171	1.001	0.630	0.091
-2.0	11.000	5.162	1.002	0.508	0.163	-4.0	11.000	5.181	1.003	0.555	0.285
-2.0	10.000	5.163	1.002	0.490	0.182	-4.0	10.000	5.174	1.001	0.536	0.149
-2.0	9.000	5.157	1.001	0.503	0.065	-4.0	9.000	5.167	1.000	0.465	0.014
-2.0	8.000	5.149	0.999	0.510	0.090	-4.0	8.000	5.170	1.001	0.515	0.072
-2.0	7.000	5.149	0.999	0.490	0.090	-4.0	7.000	5.163	0.999	0.480	0.064
-2.0	6.000	5.148	0.999	0.523	0.109	-4.0	6.000	5.167	1.000	0.480	0.014
-2.0	5.000	5.149	0.999	0.462	0.090	-4.0	5.000	5.160	0.999	0.476	0.122
-2.0	4.000	5.142	0.998	0.453	0.226	-4.0	4.000	5.165	1.000	0.480	0.025
-2.0	3.000	5.146	0.999	0.474	0.148	-4.0	3.000	5.162	0.999	0.522	0.083
-2.0	2.000	5.149	0.999	0.535	0.090	-4.0	2.000	5.163	0.999	0.430	0.064
-2.0	1.000	5.152	1.000	0.456	0.032	-4.0	1.000	5.165	1.000	0.473	0.025
-2.0	0.000	5.149	0.999	0.518	0.090	-4.0	0.000	5.168	1.000	0.438	0.033
-2.0	-1.000	5.156	1.000	0.502	0.046	-4.0	-1.000	5.163	0.999	0.480	0.064
-2.0	-2.000	5.154	1.000	0.462	0.007	-4.0	-2.000	5.167	1.000	0.581	0.014
-2.0	-3.000	5.154	1.000	0.461	0.007	-4.0	-3.000	5.162	0.999	0.513	0.083
-2.0	-4.000	5.150	0.999	0.512	0.070	-4.0	-4.000	5.164	1.000	0.521	0.044
-2.0	-5.000	5.153	1.000	0.477	0.012	-4.0	-5.000	5.165	1.000	0.472	0.025
-2.0	-6.000	5.153	1.000	0.565	0.012	-4.0	-6.000	5.164	1.000	0.500	0.044
-2.0	-7.000	5.156	1.000	0.568	0.046	-4.0	-7.000	5.166	1.000	0.422	0.006
-2.0	-8.000	5.159	1.001	0.470	0.104	-4.0	-8.000	5.154	0.998	0.471	0.238
-2.0	-9.000	5.154	1.000	0.509	0.007	-4.0	-9.000	5.171	1.001	0.498	0.091
-2.0	-10.000	5.158	1.001	0.461	0.085	-4.0	-10.000	5.166	1.000	0.542	0.006
	U ∞ =	5.154		AVG	0.080		U ∞ =	5.166		AVG	0.071

z	y	U mean	U/U ∞	T%	U var %
-6.0	11.875	4.087	0.792	9.185	20.765
-6.0	11.813	4.237	0.821	9.664	17.856
-6.0	11.750	4.430	0.859	7.971	14.115
-6.0	11.688	4.593	0.890	7.468	10.955
-6.0	11.625	4.675	0.906	6.892	9.365
-6.0	11.500	4.785	0.928	6.167	7.232
-6.0	11.375	5.007	0.971	4.415	2.928
-6.0	11.250	5.159	1.000	1.882	0.019
-6.0	11.125	5.151	0.999	1.911	0.137
-6.0	11.000	5.184	1.005	1.200	0.503
-6.0	10.000	5.177	1.004	0.550	0.368
-6.0	9.000	5.179	1.004	0.539	0.406
-6.0	8.000	5.176	1.003	0.485	0.348
-6.0	7.000	5.169	1.002	0.555	0.212
-6.0	6.000	5.156	1.000	0.455	0.040
-6.0	5.000	5.163	1.001	0.510	0.096
-6.0	4.000	5.160	1.000	0.548	0.038
-6.0	3.000	5.149	0.998	0.489	0.175
-6.0	2.000	5.146	0.998	0.499	0.233
-6.0	1.000	5.152	0.999	0.599	0.117
-6.0	0.000	5.151	0.999	0.526	0.137
-6.0	-1.000	5.157	1.000	0.543	0.020
-6.0	-2.000	5.151	0.999	0.454	0.137
-6.0	-3.000	5.153	0.999	0.561	0.098
-6.0	-4.000	5.155	0.999	0.589	0.059
-6.0	-5.000	5.147	0.998	0.544	0.214
-6.0	-6.000	5.155	0.999	0.458	0.059
-6.0	-7.000	5.145	0.997	0.566	0.253
-6.0	-8.000	5.160	1.000	0.462	0.038
-6.0	-9.000	5.150	0.998	0.467	0.156
-6.0	-10.000	5.148	0.998	0.550	0.195
	U ∞ =	5.158		AVG	0.177

Overall velocity variation at 5 m/s (%) 0.125

Average turbulence intensity at 5 m/s (%) 0.511

APPENDIX F. FLAPPING WING WAKE AT CONSTANT Z POSITION

2 ms						3ms					
z	y	U mean	U/U ∞	U RMS	T%	z	y	U mean	U/U ∞	U RMS	T%
-1.0	-9.0	2.155	1.017	0.016	0.729	-1.0	-9.0	3.076	1.002	0.018	0.582
-1.0	-8.0	2.157	1.018	0.026	1.186	-1.0	-8.0	3.075	1.001	0.019	0.607
-1.0	-7.0	2.156	1.018	0.087	4.044	-1.0	-7.0	3.075	1.001	0.025	0.823
-1.0	-6.0	2.325	1.097	0.210	9.051	-1.0	-6.0	3.074	1.001	0.050	1.615
-1.0	-5.0	2.617	1.235	0.234	8.923	-1.0	-5.0	3.493	1.138	0.143	4.613
-1.0	-4.0	2.703	1.276	0.234	8.651	-1.0	-4.0	3.208	1.045	0.435	14.112
-1.0	-3.0	2.445	1.154	0.300	12.283	-1.0	-3.0	3.239	1.055	0.357	11.012
-1.0	-2.0	2.466	1.164	0.269	10.919	-1.0	-2.0	3.345	1.089	0.340	10.180
-1.0	-1.0	2.382	1.124	0.260	10.929	-1.0	-1.0	2.966	0.966	0.322	10.859
-1.0	0.0	2.511	1.185	0.236	9.383	-1.0	0.0	2.780	0.905	0.319	11.456
-1.0	1.0	2.263	1.068	0.260	11.488	-1.0	1.0	2.978	0.970	0.342	12.318
-1.0	2.0	2.326	1.098	0.324	13.948	-1.0	2.0	3.505	1.141	0.259	10.385
-1.0	3.0	2.412	1.138	0.359	14.869	-1.0	3.0	3.706	1.207	0.363	11.799
-1.0	4.0	2.676	1.263	0.389	14.523	-1.0	4.0	3.403	1.108	0.419	12.308
-1.0	5.0	2.690	1.270	0.354	13.176	-1.0	5.0	3.173	1.033	0.376	11.836
-1.0	6.0	2.432	1.148	0.402	12.520	-1.0	6.0	3.100	1.010	0.256	8.267
-1.0	7.0	2.097	0.990	0.216	10.319	-1.0	7.0	2.991	0.974	0.106	3.555
-1.0	8.0	2.086	0.984	0.141	6.769	-1.0	8.0	2.771	0.902	0.096	3.457
-1.0	9.0	2.033	0.959	0.075	3.666	-1.0	9.0	2.989	0.973	0.097	3.232
-1.0	10.0	2.148	1.014	0.047	2.195	-1.0	10.0	3.062	0.997	0.051	1.658
	U ∞ =	2.119					U ∞ =	3.071			

THIS PAGE INTENTIONALLY LEFT BLANK

APPENDIX G. FULL MODEL WAKE AT 30 HZ AND 2 M/S

z	y	U				z	y	U			
		mean	U/U ∞	U RMS	T%			mean	U/U ∞	U RMS	T%
5.0	7.5	2.073	1.009	0.016	0.766	4.0	7.5	2.063	1.005	0.018	0.894
5.0	7.0	2.070	1.007	0.016	0.752	4.0	7.0	2.064	1.005	0.020	0.973
5.0	6.5	2.069	1.007	0.018	0.876	4.0	6.5	2.060	1.003	0.020	0.958
5.0	6.0	2.070	1.007	0.015	0.713	4.0	6.0	2.062	1.004	0.017	0.812
5.0	5.5	2.068	1.006	0.016	0.769	4.0	5.5	2.069	1.008	0.018	0.861
5.0	5.0	2.066	1.005	0.017	0.835	4.0	5.0	2.065	1.006	0.019	0.940
5.0	4.5	2.064	1.004	0.017	0.819	4.0	4.5	2.059	1.003	0.017	0.832
5.0	4.0	2.062	1.003	0.018	0.893	4.0	4.0	2.056	1.001	0.019	0.910
5.0	3.5	2.064	1.004	0.026	1.247	4.0	3.5	2.054	1.000	0.023	1.121
5.0	3.0	2.057	1.001	0.025	1.206	4.0	3.0	2.057	1.002	0.037	1.807
5.0	2.5	2.057	1.001	0.051	2.502	4.0	2.5	2.061	1.004	0.055	2.664
5.0	2.0	2.077	1.011	0.070	3.362	4.0	2.0	2.120	1.033	0.174	8.218
5.0	1.5	2.248	1.094	0.221	9.836	4.0	1.5	2.393	1.165	0.289	12.090
5.0	1.0	2.209	1.075	0.175	7.901	4.0	1.0	2.534	1.234	0.315	12.432
5.0	0.5	2.409	1.172	0.338	14.012	4.0	0.5	2.623	1.277	0.242	9.223
5.0	0.0	2.516	1.224	0.345	13.715	4.0	0.0	2.718	1.324	0.290	10.678
5.0	-0.5	2.422	1.179	0.263	10.843	4.0	-0.5	2.514	1.224	0.278	11.079
5.0	-1.0	2.264	1.102	0.174	7.700	4.0	-1.0	2.541	1.238	0.243	9.569
5.0	-1.5	2.110	1.027	0.123	5.823	4.0	-1.5	2.201	1.072	0.210	9.551
5.0	-2.0	2.080	1.012	0.126	6.055	4.0	-2.0	2.076	1.011	0.093	4.463
5.0	-2.5	2.056	1.000	0.030	1.438	4.0	-2.5	2.060	1.003	0.031	1.491
5.0	-3.0	2.053	0.999	0.030	1.448	4.0	-3.0	2.058	1.002	0.028	1.349
5.0	-3.5	2.057	1.001	0.018	0.854	4.0	-3.5	2.056	1.001	0.020	0.955
5.0	-4.0	2.053	0.999	0.022	1.063	4.0	-4.0	2.050	0.998	0.014	0.695
5.0	-4.5	2.053	0.999	0.014	0.658	4.0	-4.5	2.055	1.001	0.015	0.746
5.0	-5.0	2.050	0.998	0.014	0.667	4.0	-5.0	2.055	1.001	0.015	0.743
5.0	-5.5	2.047	0.996	0.016	0.767	4.0	-5.5	2.051	0.999	0.016	0.763
5.0	-6.0	2.045	0.995	0.015	0.734	4.0	-6.0	2.042	0.995	0.016	0.772
5.0	-6.5	2.047	0.996	0.014	0.680	4.0	-6.5	2.043	0.995	0.016	0.784
5.0	-7.0	2.042	0.994	0.016	0.802	4.0	-7.0	2.034	0.991	0.018	0.866
5.0	-7.5	2.025	0.985	0.014	0.714	4.0	-7.5	2.025	0.986	0.014	0.702
	U ∞ =	2.055					U ∞ =	2.053			

z	y	U				z	y	U			
		mean	U/U ∞	U RMS	T%			mean	U/U ∞	U RMS	T%
3.0	7.5	2.061	1.005	0.014	0.669	2.0	7.5	2.067	1.006	0.026	1.276
3.0	7.0	2.064	1.007	0.014	0.685	2.0	7.0	2.074	1.010	0.021	1.016
3.0	6.5	2.067	1.008	0.014	0.679	2.0	6.5	2.062	1.004	0.019	0.911
3.0	6.0	2.066	1.008	0.017	0.800	2.0	6.0	2.061	1.003	0.036	1.755
3.0	5.5	2.068	1.009	0.016	0.789	2.0	5.5	2.075	1.010	0.045	2.183
3.0	5.0	2.070	1.010	0.016	0.795	2.0	5.0	2.090	1.017	0.069	3.316
3.0	4.5	2.068	1.009	0.018	0.889	2.0	4.5	2.082	1.014	0.053	2.535
3.0	4.0	2.068	1.009	0.017	0.813	2.0	4.0	2.067	1.006	0.031	1.488
3.0	3.5	2.051	1.000	0.019	0.910	2.0	3.5	2.055	1.000	0.048	2.353
3.0	3.0	2.056	1.003	0.020	0.970	2.0	3.0	2.049	0.998	0.041	1.997
3.0	2.5	2.057	1.003	0.046	2.239	2.0	2.5	2.051	0.998	0.036	1.748
3.0	2.0	2.126	1.037	0.152	7.160	2.0	2.0	2.049	0.998	0.050	2.422
3.0	1.5	2.197	1.072	0.240	10.909	2.0	1.5	2.067	1.006	0.119	5.741
3.0	1.0	2.398	1.170	0.265	11.064	2.0	1.0	2.383	1.160	0.392	16.450
3.0	0.5	2.817	1.374	0.315	11.170	2.0	0.5	2.426	1.181	0.340	14.004
3.0	0.0	2.604	1.270	0.353	13.559	2.0	0.0	2.767	1.347	0.350	12.645
3.0	-0.5	2.619	1.278	0.282	10.763	2.0	-0.5	2.663	1.296	0.346	13.003
3.0	-1.0	2.424	1.182	0.291	12.003	2.0	-1.0	2.202	1.072	0.239	10.830
3.0	-1.5	2.115	1.032	0.148	6.996	2.0	-1.5	2.071	1.008	0.126	6.082
3.0	-2.0	2.054	1.002	0.042	2.033	2.0	-2.0	2.074	1.010	0.137	6.605
3.0	-2.5	2.048	0.999	0.043	2.093	2.0	-2.5	2.047	0.997	0.031	1.522
3.0	-3.0	2.049	1.000	0.029	1.396	2.0	-3.0	2.054	1.000	0.026	1.272
3.0	-3.5	2.051	1.000	0.027	1.332	2.0	-3.5	2.059	1.002	0.035	1.704
3.0	-4.0	2.047	0.999	0.018	0.903	2.0	-4.0	2.063	1.004	0.023	1.104
3.0	-4.5	2.050	1.000	0.017	0.808	2.0	-4.5	2.055	1.000	0.019	0.916
3.0	-5.0	2.046	0.998	0.017	0.810	2.0	-5.0	2.060	1.003	0.032	1.554
3.0	-5.5	2.047	0.999	0.016	0.768	2.0	-5.5	2.053	0.999	0.027	1.321
3.0	-6.0	2.042	0.996	0.015	0.744	2.0	-6.0	2.047	0.997	0.021	1.004
3.0	-6.5	2.035	0.993	0.013	0.659	2.0	-6.5	2.041	0.994	0.016	0.785
3.0	-7.0	2.031	0.991	0.016	0.766	2.0	-7.0	2.032	0.989	0.014	0.690
3.0	-7.5	2.023	0.987	0.016	0.792	2.0	-7.5	2.023	0.985	0.014	0.701
	U ∞ =	2.050					U ∞ =	2.054			

z	y	U				z	y	U			
		mean	U/U ∞	U RMS	T%			mean	U/U ∞	U RMS	T%
1.0	7.5	2.136	1.042	0.140	6.568	0.0	7.5	2.064	1.018	0.094	4.540
1.0	7.0	2.169	1.058	0.131	6.023	0.0	7.0	2.088	1.029	0.146	6.992
1.0	6.5	2.086	1.018	0.107	5.121	0.0	6.5	2.036	1.004	0.126	6.199
1.0	6.0	2.089	1.019	0.116	5.576	0.0	6.0	1.978	0.975	0.133	6.703
1.0	5.5	2.072	1.011	0.141	6.809	0.0	5.5	2.017	0.994	0.075	3.720
1.0	5.0	2.071	1.010	0.111	5.346	0.0	5.0	1.980	0.976	0.112	5.669
1.0	4.5	2.086	1.018	0.127	6.102	0.0	4.5	2.042	1.007	0.084	4.132
1.0	4.0	2.154	1.051	0.123	5.706	0.0	4.0	2.132	1.051	0.119	5.564
1.0	3.5	2.173	1.060	0.100	4.613	0.0	3.5	2.198	1.084	0.100	4.559
1.0	3.0	2.216	1.081	0.165	7.456	0.0	3.0	2.191	1.080	0.118	5.371
1.0	2.5	2.136	1.042	0.154	7.188	0.0	2.5	2.176	1.073	0.163	7.515
1.0	2.0	2.035	0.993	0.128	6.278	0.0	2.0	2.200	1.085	0.117	5.335
1.0	1.5	2.062	1.006	0.180	8.749	0.0	1.5	2.094	1.032	0.200	9.574
1.0	1.0	2.050	1.000	0.208	10.153	0.0	1.0	2.047	1.009	0.257	12.536
1.0	0.5	2.439	1.190	0.313	12.825	0.0	0.5	2.361	1.164	0.311	13.186
1.0	0.0	2.839	1.385	0.326	11.488	0.0	0.0	2.669	1.316	0.309	11.574
1.0	-0.5	2.611	1.274	0.403	15.424	0.0	-0.5	2.394	1.180	0.235	9.801
1.0	-1.0	2.187	1.067	0.243	11.111	0.0	-1.0	2.095	1.033	0.242	11.536
1.0	-1.5	2.047	0.999	0.113	5.514	0.0	-1.5	1.974	0.973	0.145	7.350
1.0	-2.0	2.054	1.002	0.070	3.407	0.0	-2.0	2.059	1.015	0.091	4.398
1.0	-2.5	2.069	1.009	0.077	3.727	0.0	-2.5	2.093	1.032	0.171	8.192
1.0	-3.0	2.092	1.020	0.109	5.225	0.0	-3.0	2.217	1.093	0.165	7.427
1.0	-3.5	2.078	1.014	0.075	3.587	0.0	-3.5	2.221	1.095	0.160	7.217
1.0	-4.0	2.115	1.032	0.087	4.113	0.0	-4.0	2.116	1.043	0.172	8.131
1.0	-4.5	2.095	1.022	0.129	6.166	0.0	-4.5	2.137	1.054	0.181	8.485
1.0	-5.0	2.065	1.007	0.124	6.011	0.0	-5.0	2.137	1.054	0.170	7.978
1.0	-5.5	2.053	1.001	0.147	7.178	0.0	-5.5	2.025	0.998	0.104	5.160
1.0	-6.0	2.108	1.028	0.136	6.469	0.0	-6.0	2.044	1.008	0.092	4.490
1.0	-6.5	2.055	1.002	0.067	3.246	0.0	-6.5	2.073	1.022	0.130	6.250
1.0	-7.0	2.044	0.997	0.040	1.957	0.0	-7.0	1.999	0.986	0.024	1.206
1.0	-7.5	2.007	0.979	0.017	0.865	0.0	-7.5	1.994	0.983	0.021	1.061
	U ∞ =	2.050					U ∞ =	2.028			

z	y	U mean	U/U ∞	U RMS	T%	z	y	U mean	U/U ∞	U RMS	T%
-1.0	7.5	2.064	1.010	0.050	2.436	-2.0	7.5	2.086	1.002	0.017	0.837
-1.0	7.0	2.082	1.018	0.071	3.418	-2.0	7.0	2.092	1.005	0.019	0.919
-1.0	6.5	2.064	1.010	0.065	3.128	-2.0	6.5	2.091	1.005	0.027	1.296
-1.0	6.0	2.044	1.000	0.074	3.632	-2.0	6.0	2.095	1.007	0.019	0.916
-1.0	5.5	2.033	0.994	0.075	3.693	-2.0	5.5	2.085	1.002	0.041	1.968
-1.0	5.0	2.061	1.008	0.063	3.043	-2.0	5.0	2.098	1.008	0.044	2.089
-1.0	4.5	2.070	1.012	0.090	4.340	-2.0	4.5	2.086	1.002	0.065	3.129
-1.0	4.0	2.091	1.023	0.067	3.204	-2.0	4.0	2.096	1.007	0.129	6.143
-1.0	3.5	2.119	1.036	0.149	7.038	-2.0	3.5	2.177	1.046	0.184	8.464
-1.0	3.0	2.275	1.113	0.239	10.507	-2.0	3.0	2.356	1.132	0.223	9.448
-1.0	2.5	2.225	1.088	0.234	10.509	-2.0	2.5	2.551	1.226	0.250	9.815
-1.0	2.0	2.165	1.059	0.190	8.794	-2.0	2.0	2.413	1.159	0.255	10.561
-1.0	1.5	2.036	0.996	0.226	11.085	-2.0	1.5	2.249	1.080	0.303	13.458
-1.0	1.0	2.179	1.066	0.302	13.873	-2.0	1.0	2.389	1.148	0.272	11.367
-1.0	0.5	2.342	1.146	0.331	14.149	-2.0	0.5	2.662	1.279	0.293	10.999
-1.0	0.0	2.661	1.302	0.364	13.664	-2.0	0.0	2.624	1.261	0.303	11.560
-1.0	-0.5	2.530	1.237	0.309	12.194	-2.0	-0.5	2.285	1.098	0.274	12.002
-1.0	-1.0	2.071	1.013	0.218	10.530	-2.0	-1.0	2.276	1.093	0.219	9.629
-1.0	-1.5	2.074	1.014	0.208	10.043	-2.0	-1.5	2.207	1.060	0.268	12.151
-1.0	-2.0	2.206	1.079	0.221	10.024	-2.0	-2.0	2.374	1.141	0.267	11.267
-1.0	-2.5	2.201	1.077	0.198	8.985	-2.0	-2.5	2.294	1.102	0.247	10.769
-1.0	-3.0	2.252	1.101	0.179	7.945	-2.0	-3.0	2.147	1.031	0.172	8.024
-1.0	-3.5	2.203	1.078	0.180	8.191	-2.0	-3.5	2.173	1.044	0.151	6.946
-1.0	-4.0	2.114	1.034	0.112	5.298	-2.0	-4.0	2.145	1.031	0.135	6.287
-1.0	-4.5	2.162	1.057	0.173	8.011	-2.0	-4.5	2.124	1.020	0.135	6.362
-1.0	-5.0	2.059	1.007	0.177	8.612	-2.0	-5.0	2.078	0.998	0.135	6.474
-1.0	-5.5	2.068	1.011	0.145	7.016	-2.0	-5.5	2.125	1.021	0.141	6.652
-1.0	-6.0	2.062	1.009	0.091	4.394	-2.0	-6.0	2.098	1.008	0.077	3.669
-1.0	-6.5	2.044	1.000	0.139	6.801	-2.0	-6.5	2.080	0.999	0.066	3.159
-1.0	-7.0	2.015	0.986	0.043	2.126	-2.0	-7.0	2.057	0.988	0.031	1.494
-1.0	-7.5	2.010	0.983	0.022	1.074	-2.0	-7.5	2.049	0.984	0.019	0.934
	U ∞ =	2.045					U ∞ =	2.081			

z	y	U mean	U/U ∞	U RMS	T%	z	y	U mean	U/U ∞	U RMS	T%
-3.0	7.5	2.089	1.005	0.015	0.715	-4.0	7.5	2.086	1.004	0.026	1.226
-3.0	7.0	2.097	1.009	0.019	0.902	-4.0	7.0	2.118	1.020	0.029	1.384
-3.0	6.5	2.101	1.011	0.023	1.086	-4.0	6.5	2.125	1.023	0.042	1.967
-3.0	6.0	2.102	1.011	0.024	1.119	-4.0	6.0	2.134	1.027	0.048	2.238
-3.0	5.5	2.115	1.017	0.028	1.344	-4.0	5.5	2.134	1.027	0.022	1.035
-3.0	5.0	2.120	1.020	0.029	1.383	-4.0	5.0	2.139	1.030	0.031	1.445
-3.0	4.5	2.107	1.013	0.071	3.384	-4.0	4.5	2.126	1.024	0.061	2.860
-3.0	4.0	2.094	1.007	0.135	6.436	-4.0	4.0	2.105	1.013	0.092	4.365
-3.0	3.5	2.099	1.010	0.127	6.073	-4.0	3.5	2.044	0.984	0.193	9.445
-3.0	3.0	2.120	1.020	0.169	7.953	-4.0	3.0	2.093	1.008	0.161	7.696
-3.0	2.5	2.410	1.159	0.248	10.293	-4.0	2.5	2.143	1.032	0.140	6.546
-3.0	2.0	2.549	1.226	0.234	9.178	-4.0	2.0	2.271	1.093	0.179	7.890
-3.0	1.5	2.394	1.151	0.221	9.243	-4.0	1.5	2.244	1.080	0.249	11.087
-3.0	1.0	2.419	1.163	0.257	10.629	-4.0	1.0	2.228	1.073	0.202	9.076
-3.0	0.5	2.468	1.187	0.237	9.613	-4.0	0.5	2.241	1.079	0.247	11.032
-3.0	0.0	2.556	1.229	0.297	11.628	-4.0	0.0	2.264	1.090	0.295	13.037
-3.0	-0.5	2.592	1.247	0.314	12.095	-4.0	-0.5	2.159	1.039	0.227	10.511
-3.0	-1.0	2.458	1.182	0.238	9.694	-4.0	-1.0	2.129	1.025	0.257	12.061
-3.0	-1.5	2.433	1.170	0.214	8.800	-4.0	-1.5	2.103	1.012	0.193	9.184
-3.0	-2.0	2.372	1.141	0.295	12.434	-4.0	-2.0	2.130	1.025	0.222	10.401
-3.0	-2.5	2.182	1.049	0.215	9.832	-4.0	-2.5	2.128	1.024	0.150	7.059
-3.0	-3.0	2.213	1.064	0.182	8.222	-4.0	-3.0	2.083	1.003	0.184	8.828
-3.0	-3.5	2.128	1.023	0.154	7.236	-4.0	-3.5	2.096	1.009	0.158	7.553
-3.0	-4.0	2.182	1.049	0.174	7.976	-4.0	-4.0	2.170	1.045	0.081	3.749
-3.0	-4.5	2.131	1.025	0.095	4.477	-4.0	-4.5	2.136	1.028	0.041	1.940
-3.0	-5.0	2.121	1.020	0.087	4.096	-4.0	-5.0	2.125	1.023	0.077	3.642
-3.0	-5.5	2.101	1.011	0.074	3.523	-4.0	-5.5	2.087	1.005	0.041	1.969
-3.0	-6.0	2.096	1.008	0.041	1.934	-4.0	-6.0	2.091	1.007	0.030	1.418
-3.0	-6.5	2.076	0.998	0.027	1.281	-4.0	-6.5	2.059	0.991	0.051	2.473
-3.0	-7.0	2.065	0.993	0.020	0.970	-4.0	-7.0	2.058	0.991	0.018	0.863
-3.0	-7.5	2.052	0.987	0.018	0.867	-4.0	-7.5	2.041	0.983	0.021	1.035
	U ∞ =	2.079					U ∞ =	2.077			

z	y	U		U	
		mean	U/U ∞	RMS	T%
-5.0	7.5	1.992	0.984	0.102	5.122
-5.0	7.0	2.004	0.989	0.103	5.116
-5.0	6.5	2.084	1.029	0.121	5.786
-5.0	6.0	2.095	1.034	0.142	6.763
-5.0	5.5	2.134	1.054	0.122	5.739
-5.0	5.0	2.147	1.060	0.127	5.923
-5.0	4.5	2.140	1.057	0.111	5.180
-5.0	4.0	2.127	1.050	0.137	6.443
-5.0	3.5	2.160	1.066	0.195	9.042
-5.0	3.0	2.050	1.012	0.215	10.503
-5.0	2.5	2.082	1.028	0.210	10.102
-5.0	2.0	2.125	1.049	0.274	12.905
-5.0	1.5	2.478	1.224	0.326	13.142
-5.0	1.0	2.391	1.181	0.382	15.975
-5.0	0.5	2.622	1.295	0.301	11.470
-5.0	0.0	2.643	1.305	0.320	12.110
-5.0	-0.5	2.404	1.187	0.323	13.422
-5.0	-1.0	2.096	1.035	0.257	12.268
-5.0	-1.5	2.145	1.059	0.265	12.353
-5.0	-2.0	2.106	1.040	0.228	10.802
-5.0	-2.5	2.112	1.043	0.196	9.264
-5.0	-3.0	2.017	0.996	0.175	8.662
-5.0	-3.5	2.083	1.028	0.121	5.796
-5.0	-4.0	2.124	1.049	0.149	7.021
-5.0	-4.5	2.155	1.064	0.138	6.412
-5.0	-5.0	2.123	1.048	0.120	5.639
-5.0	-5.5	2.040	1.007	0.128	6.293
-5.0	-6.0	2.012	0.993	0.111	5.510
-5.0	-6.5	2.027	1.001	0.073	3.583
-5.0	-7.0	1.956	0.966	0.120	6.158
-5.0	-7.5	2.018	0.996	0.052	2.555
	U ∞ =	2.025			

APPENDIX H. FULL MODEL WAKE AT 30 HZ AND 3 M/S

z	y	U				z	y	U			
		mean	U/U ∞	U RMS	T%			mean	U/U ∞	U RMS	T%
5.0	7.5	3.032	1.007	0.016	0.529	4.0	7.5	3.044	1.011	0.018	0.600
5.0	7.0	3.026	1.005	0.015	0.501	4.0	7.0	3.051	1.014	0.014	0.469
5.0	6.5	3.045	1.012	0.015	0.490	4.0	6.5	3.064	1.018	0.016	0.512
5.0	6.0	3.044	1.011	0.022	0.716	4.0	6.0	3.063	1.018	0.018	0.581
5.0	5.5	3.046	1.012	0.017	0.545	4.0	5.5	3.050	1.013	0.018	0.594
5.0	5.0	3.049	1.013	0.018	0.584	4.0	5.0	3.036	1.009	0.016	0.538
5.0	4.5	3.047	1.012	0.019	0.631	4.0	4.5	3.042	1.011	0.020	0.645
5.0	4.0	3.051	1.014	0.015	0.495	4.0	4.0	3.034	1.008	0.016	0.537
5.0	3.5	3.024	1.005	0.027	0.904	4.0	3.5	3.036	1.009	0.029	0.966
5.0	3.0	3.020	1.003	0.023	0.776	4.0	3.0	3.039	1.010	0.026	0.844
5.0	2.5	3.019	1.003	0.026	0.857	4.0	2.5	3.032	1.007	0.023	0.744
5.0	2.0	3.018	1.003	0.026	0.850	4.0	2.0	3.035	1.008	0.029	0.948
5.0	1.5	3.022	1.004	0.025	0.835	4.0	1.5	3.018	1.003	0.086	2.860
5.0	1.0	3.019	1.003	0.043	1.434	4.0	1.0	3.093	1.028	0.150	4.841
5.0	0.5	3.030	1.007	0.041	1.355	4.0	0.5	3.206	1.065	0.212	6.602
5.0	0.0	3.010	1.000	0.092	3.060	4.0	0.0	3.190	1.060	0.227	7.112
5.0	-0.5	3.012	1.001	0.084	2.791	4.0	-0.5	3.095	1.028	0.194	6.268
5.0	-1.0	3.025	1.005	0.041	1.342	4.0	-1.0	3.078	1.023	0.185	6.018
5.0	-1.5	3.018	1.003	0.028	0.936	4.0	-1.5	3.069	1.020	0.151	4.909
5.0	-2.0	3.019	1.003	0.022	0.722	4.0	-2.0	3.035	1.008	0.048	1.589
5.0	-2.5	3.012	1.001	0.017	0.575	4.0	-2.5	3.028	1.006	0.023	0.767
5.0	-3.0	3.019	1.003	0.017	0.567	4.0	-3.0	3.033	1.008	0.019	0.615
5.0	-3.5	3.017	1.002	0.019	0.615	4.0	-3.5	3.036	1.009	0.015	0.505
5.0	-4.0	3.018	1.003	0.019	0.616	4.0	-4.0	3.032	1.007	0.015	0.510
5.0	-4.5	3.017	1.002	0.016	0.544	4.0	-4.5	3.023	1.004	0.018	0.595
5.0	-5.0	3.010	1.000	0.018	0.587	4.0	-5.0	3.021	1.004	0.015	0.510
5.0	-5.5	3.011	1.000	0.018	0.605	4.0	-5.5	3.017	1.002	0.020	0.677
5.0	-6.0	3.010	1.000	0.016	0.539	4.0	-6.0	3.013	1.001	0.016	0.527
5.0	-6.5	3.003	0.998	0.017	0.578	4.0	-6.5	3.013	1.001	0.018	0.593
5.0	-7.0	2.993	0.994	0.017	0.557	4.0	-7.0	2.996	0.995	0.019	0.644
5.0	-7.5	2.987	0.992	0.018	0.607	4.0	-7.5	2.989	0.993	0.016	0.526
	U ∞ =	3.010					U ∞ =	3.010			

z	y	U				T%	z	y	U				T%
		mean	U/U ∞	U	RMS				mean	U/U ∞	U	RMS	
3.0	7.5	3.075	1.022	0.018	0.600	2.0	7.5	3.063	1.018	0.018	0.589		
3.0	7.0	3.045	1.012	0.021	0.693	2.0	7.0	3.061	1.017	0.021	0.681		
3.0	6.5	3.040	1.010	0.021	0.689	2.0	6.5	3.067	1.019	0.023	0.754		
3.0	6.0	3.043	1.011	0.018	0.602	2.0	6.0	3.063	1.018	0.038	1.229		
3.0	5.5	3.064	1.018	0.017	0.558	2.0	5.5	3.081	1.024	0.085	2.751		
3.0	5.0	3.040	1.010	0.026	0.851	2.0	5.0	3.062	1.017	0.130	4.241		
3.0	4.5	3.059	1.016	0.027	0.871	2.0	4.5	3.058	1.016	0.159	5.189		
3.0	4.0	3.047	1.012	0.041	1.334	2.0	4.0	3.107	1.032	0.120	3.855		
3.0	3.5	3.038	1.009	0.024	0.792	2.0	3.5	3.051	1.014	0.151	4.948		
3.0	3.0	3.038	1.009	0.032	1.060	2.0	3.0	3.087	1.026	0.133	4.298		
3.0	2.5	3.037	1.009	0.028	0.938	2.0	2.5	3.029	1.006	0.066	2.186		
3.0	2.0	3.024	1.005	0.074	2.458	2.0	2.0	3.034	1.008	0.104	3.431		
3.0	1.5	3.036	1.009	0.133	4.393	2.0	1.5	3.057	1.016	0.101	3.292		
3.0	1.0	3.327	1.105	0.325	9.772	2.0	1.0	3.102	1.031	0.216	6.959		
3.0	0.5	3.451	1.147	0.351	10.163	2.0	0.5	3.497	1.162	0.276	7.895		
3.0	0.0	3.563	1.184	0.324	9.082	2.0	0.0	3.645	1.211	0.348	9.544		
3.0	-0.5	3.444	1.144	0.286	8.315	2.0	-0.5	3.504	1.164	0.374	10.665		
3.0	-1.0	3.288	1.092	0.254	7.736	2.0	-1.0	3.272	1.087	0.306	9.366		
3.0	-1.5	3.052	1.014	0.211	6.899	2.0	-1.5	3.071	1.020	0.137	4.466		
3.0	-2.0	3.035	1.008	0.038	1.265	2.0	-2.0	3.033	1.008	0.064	2.118		
3.0	-2.5	3.037	1.009	0.018	0.586	2.0	-2.5	3.034	1.008	0.043	1.404		
3.0	-3.0	3.029	1.006	0.017	0.567	2.0	-3.0	3.027	1.006	0.088	2.895		
3.0	-3.5	3.025	1.005	0.025	0.815	2.0	-3.5	3.045	1.012	0.064	2.112		
3.0	-4.0	3.034	1.008	0.018	0.586	2.0	-4.0	3.051	1.014	0.086	2.824		
3.0	-4.5	3.030	1.007	0.018	0.609	2.0	-4.5	3.049	1.013	0.068	2.217		
3.0	-5.0	3.031	1.007	0.020	0.662	2.0	-5.0	3.033	1.008	0.076	2.517		
3.0	-5.5	3.025	1.005	0.017	0.563	2.0	-5.5	3.049	1.013	0.069	2.255		
3.0	-6.0	3.014	1.001	0.020	0.647	2.0	-6.0	3.010	1.000	0.044	1.471		
3.0	-6.5	3.009	1.000	0.020	0.675	2.0	-6.5	3.012	1.001	0.023	0.768		
3.0	-7.0	2.999	0.996	0.017	0.574	2.0	-7.0	3.004	0.998	0.018	0.584		
3.0	-7.5	2.985	0.992	0.016	0.535	2.0	-7.5	2.984	0.991	0.019	0.621		
	U ∞ =	3.010					U ∞ =	3.010					

z	y	U				z	y	U			
		mean	U/U ∞	U RMS	T%			mean	U/U ∞	U RMS	T%
1.0	7.5	3.064	1.018	0.026	0.856	0.0	7.5	3.067	1.019	0.035	1.134
1.0	7.0	3.073	1.021	0.080	2.619	0.0	7.0	3.084	1.025	0.066	2.154
1.0	6.5	3.120	1.037	0.139	4.452	0.0	6.5	3.137	1.042	0.212	6.770
1.0	6.0	3.251	1.080	0.229	7.039	0.0	6.0	3.227	1.072	0.219	6.771
1.0	5.5	3.215	1.068	0.202	6.270	0.0	5.5	3.186	1.058	0.220	6.900
1.0	5.0	3.069	1.020	0.243	7.910	0.0	5.0	3.048	1.013	0.168	5.519
1.0	4.5	2.980	0.990	0.230	7.727	0.0	4.5	2.810	0.934	0.250	8.899
1.0	4.0	2.948	0.979	0.241	8.159	0.0	4.0	2.871	0.954	0.294	10.237
1.0	3.5	2.824	0.938	0.190	6.742	0.0	3.5	3.085	1.025	0.321	10.417
1.0	3.0	2.815	0.935	0.234	8.321	0.0	3.0	2.998	0.996	0.380	12.672
1.0	2.5	2.996	0.995	0.166	5.540	0.0	2.5	2.908	0.966	0.244	8.389
1.0	2.0	3.066	1.019	0.106	3.444	0.0	2.0	2.986	0.992	0.220	7.359
1.0	1.5	3.027	1.006	0.116	3.842	0.0	1.5	3.165	1.051	0.200	6.326
1.0	1.0	3.281	1.090	0.268	8.174	0.0	1.0	3.401	1.130	0.242	7.105
1.0	0.5	3.437	1.142	0.327	9.527	0.0	0.5	3.402	1.130	0.367	10.775
1.0	0.0	3.538	1.175	0.407	11.502	0.0	0.0	3.255	1.081	0.325	9.992
1.0	-0.5	3.536	1.175	0.375	10.605	0.0	-0.5	3.207	1.065	0.371	11.571
1.0	-1.0	3.069	1.020	0.206	6.705	0.0	-1.0	3.234	1.074	0.263	8.133
1.0	-1.5	3.022	1.004	0.110	3.630	0.0	-1.5	3.047	1.012	0.234	7.690
1.0	-2.0	3.051	1.014	0.109	3.584	0.0	-2.0	2.936	0.975	0.211	7.178
1.0	-2.5	3.028	1.006	0.143	4.735	0.0	-2.5	2.955	0.982	0.225	7.611
1.0	-3.0	3.002	0.997	0.210	6.988	0.0	-3.0	3.054	1.015	0.269	8.822
1.0	-3.5	3.048	1.013	0.195	6.402	0.0	-3.5	3.148	1.046	0.253	8.041
1.0	-4.0	2.983	0.991	0.159	5.324	0.0	-4.0	3.041	1.010	0.335	11.003
1.0	-4.5	3.057	1.016	0.211	6.894	0.0	-4.5	2.944	0.978	0.229	7.761
1.0	-5.0	3.216	1.068	0.244	7.590	0.0	-5.0	3.074	1.021	0.282	9.185
1.0	-5.5	3.247	1.079	0.206	6.352	0.0	-5.5	3.211	1.067	0.219	6.822
1.0	-6.0	3.061	1.017	0.126	4.130	0.0	-6.0	3.168	1.052	0.237	7.477
1.0	-6.5	3.002	0.997	0.043	1.434	0.0	-6.5	3.007	0.999	0.070	2.334
1.0	-7.0	3.006	0.999	0.024	0.809	0.0	-7.0	2.998	0.996	0.031	1.031
1.0	-7.5	2.988	0.993	0.016	0.551	0.0	-7.5	2.988	0.993	0.022	0.726
	U ∞ =	3.010					U ∞ =	3.010			

z	y	U		U		z	y	U		U	
		mean	U/U ∞	RMS	T%			mean	U/U ∞	RMS	T%
-1.0	7.5	3.065	1.018	0.018	0.597	-2.0	7.5	3.075	1.022	0.019	0.622
-1.0	7.0	3.064	1.018	0.030	0.966	-2.0	7.0	3.073	1.021	0.022	0.711
-1.0	6.5	3.075	1.022	0.093	3.009	-2.0	6.5	3.065	1.018	0.042	1.369
-1.0	6.0	3.113	1.034	0.111	3.560	-2.0	6.0	3.077	1.022	0.043	1.405
-1.0	5.5	3.123	1.038	0.203	6.509	-2.0	5.5	3.112	1.034	0.147	4.712
-1.0	5.0	3.001	0.997	0.253	8.447	-2.0	5.0	3.100	1.030	0.178	5.757
-1.0	4.5	2.918	0.969	0.314	10.748	-2.0	4.5	3.080	1.023	0.252	8.176
-1.0	4.0	2.906	0.965	0.417	14.355	-2.0	4.0	3.115	1.035	0.321	10.319
-1.0	3.5	3.305	1.098	0.335	10.141	-2.0	3.5	2.767	0.919	0.372	13.444
-1.0	3.0	3.247	1.079	0.336	10.349	-2.0	3.0	2.750	0.914	0.432	15.714
-1.0	2.5	3.399	1.129	0.357	10.492	-2.0	2.5	2.969	0.986	0.368	12.408
-1.0	2.0	3.273	1.087	0.371	11.327	-2.0	2.0	2.954	0.981	0.372	12.581
-1.0	1.5	3.366	1.118	0.306	9.081	-2.0	1.5	3.079	1.023	0.359	11.645
-1.0	1.0	3.223	1.071	0.290	9.011	-2.0	1.0	2.914	0.968	0.346	11.867
-1.0	0.5	3.114	1.035	0.339	10.872	-2.0	0.5	2.664	0.885	0.253	9.502
-1.0	0.0	2.906	0.965	0.283	9.726	-2.0	0.0	2.627	0.873	0.283	10.770
-1.0	-0.5	2.917	0.969	0.244	8.355	-2.0	-0.5	2.663	0.885	0.393	14.755
-1.0	-1.0	3.102	1.031	0.332	10.691	-2.0	-1.0	2.613	0.868	0.345	13.186
-1.0	-1.5	3.197	1.062	0.315	9.844	-2.0	-1.5	3.009	1.000	0.388	12.909
-1.0	-2.0	3.073	1.021	0.332	10.789	-2.0	-2.0	3.063	1.018	0.325	10.611
-1.0	-2.5	3.252	1.080	0.362	11.130	-2.0	-2.5	3.061	1.017	0.398	13.019
-1.0	-3.0	3.281	1.090	0.386	11.761	-2.0	-3.0	2.908	0.966	0.359	12.347
-1.0	-3.5	3.014	1.001	0.414	13.730	-2.0	-3.5	2.941	0.977	0.316	10.748
-1.0	-4.0	2.909	0.966	0.317	10.879	-2.0	-4.0	3.048	1.013	0.300	9.848
-1.0	-4.5	2.870	0.953	0.318	11.082	-2.0	-4.5	3.227	1.072	0.287	8.903
-1.0	-5.0	3.108	1.033	0.270	8.672	-2.0	-5.0	3.237	1.075	0.330	10.197
-1.0	-5.5	3.211	1.067	0.277	8.627	-2.0	-5.5	3.221	1.070	0.314	9.761
-1.0	-6.0	3.078	1.023	0.189	6.134	-2.0	-6.0	3.030	1.007	0.140	4.607
-1.0	-6.5	3.026	1.005	0.060	1.998	-2.0	-6.5	3.009	1.000	0.053	1.777
-1.0	-7.0	3.003	0.998	0.041	1.379	-2.0	-7.0	3.003	0.998	0.024	0.814
-1.0	-7.5	2.990	0.993	0.020	0.669	-2.0	-7.5	2.988	0.993	0.021	0.689
	U ∞ =	3.010					U ∞ =	3.010			

z	y	U mean	U/U ∞	U RMS	T%	z	y	U mean	U/U ∞	U RMS	T%
-3.0	7.5	3.072	1.021	0.020	0.651	-4.0	7.5	3.079	1.023	0.019	0.610
-3.0	7.0	3.075	1.022	0.018	0.596	-4.0	7.0	3.083	1.024	0.017	0.538
-3.0	6.5	3.083	1.024	0.022	0.727	-4.0	6.5	3.095	1.028	0.022	0.709
-3.0	6.0	3.077	1.022	0.087	2.819	-4.0	6.0	3.089	1.026	0.052	1.691
-3.0	5.5	3.074	1.021	0.073	2.376	-4.0	5.5	3.089	1.026	0.100	3.247
-3.0	5.0	3.071	1.020	0.133	4.318	-4.0	5.0	3.120	1.037	0.095	3.051
-3.0	4.5	3.113	1.034	0.187	6.015	-4.0	4.5	3.128	1.039	0.163	5.212
-3.0	4.0	3.236	1.075	0.294	9.097	-4.0	4.0	3.125	1.038	0.242	7.747
-3.0	3.5	3.109	1.033	0.302	9.717	-4.0	3.5	3.115	1.035	0.321	10.315
-3.0	3.0	2.891	0.960	0.306	10.584	-4.0	3.0	3.000	0.997	0.378	12.606
-3.0	2.5	2.770	0.920	0.272	9.807	-4.0	2.5	2.892	0.961	0.288	9.971
-3.0	2.0	2.777	0.923	0.314	11.303	-4.0	2.0	3.067	1.019	0.395	12.892
-3.0	1.5	2.770	0.920	0.315	11.386	-4.0	1.5	3.139	1.043	0.396	12.607
-3.0	1.0	2.796	0.929	0.332	11.880	-4.0	1.0	3.071	1.020	0.334	10.869
-3.0	0.5	2.842	0.944	0.344	12.118	-4.0	0.5	3.096	1.029	0.448	14.480
-3.0	0.0	2.879	0.956	0.286	9.947	-4.0	0.0	3.263	1.084	0.402	12.333
-3.0	-0.5	2.816	0.936	0.245	8.700	-4.0	-0.5	3.095	1.028	0.392	12.652
-3.0	-1.0	2.791	0.927	0.284	10.183	-4.0	-1.0	3.306	1.098	0.419	12.667
-3.0	-1.5	2.583	0.858	0.269	10.433	-4.0	-1.5	2.960	0.983	0.397	13.428
-3.0	-2.0	2.649	0.880	0.321	12.134	-4.0	-2.0	2.957	0.982	0.362	12.231
-3.0	-2.5	2.601	0.864	0.240	9.239	-4.0	-2.5	2.885	0.958	0.275	9.533
-3.0	-3.0	2.929	0.973	0.288	9.845	-4.0	-3.0	3.066	1.019	0.316	10.298
-3.0	-3.5	3.196	1.062	0.342	10.686	-4.0	-3.5	3.085	1.025	0.233	7.568
-3.0	-4.0	3.238	1.076	0.252	7.769	-4.0	-4.0	3.093	1.028	0.269	8.688
-3.0	-4.5	3.136	1.042	0.240	7.660	-4.0	-4.5	3.057	1.016	0.184	6.004
-3.0	-5.0	3.109	1.033	0.345	11.112	-4.0	-5.0	3.052	1.014	0.098	3.220
-3.0	-5.5	3.025	1.005	0.243	8.037	-4.0	-5.5	3.049	1.013	0.046	1.516
-3.0	-6.0	3.033	1.008	0.119	3.928	-4.0	-6.0	3.032	1.007	0.033	1.076
-3.0	-6.5	3.023	1.004	0.036	1.175	-4.0	-6.5	3.036	1.009	0.026	0.843
-3.0	-7.0	3.003	0.998	0.023	0.765	-4.0	-7.0	3.015	1.002	0.021	0.681
-3.0	-7.5	2.999	0.996	0.022	0.738	-4.0	-7.5	3.002	0.997	0.017	0.562
	U ∞ =	3.010					U ∞ =	3.010			

z	y	U		U	
		mean	U/U ∞	RMS	T%
-5.0	7.5	3.112	1.034	0.025	0.793
-5.0	7.0	3.103	1.031	0.023	0.751
-5.0	6.5	3.114	1.035	0.028	0.900
-5.0	6.0	3.069	1.020	0.074	2.407
-5.0	5.5	3.107	1.032	0.149	4.784
-5.0	5.0	3.147	1.046	0.250	7.950
-5.0	4.5	3.334	1.108	0.341	10.218
-5.0	4.0	3.326	1.105	0.397	11.943
-5.0	3.5	3.161	1.050	0.406	12.836
-5.0	3.0	3.009	1.000	0.381	12.657
-5.0	2.5	3.252	1.080	0.504	15.496
-5.0	2.0	3.268	1.086	0.398	12.165
-5.0	1.5	3.465	1.151	0.443	12.785
-5.0	1.0	3.391	1.127	0.424	12.514
-5.0	0.5	3.469	1.152	0.433	12.473
-5.0	0.0	3.658	1.215	0.473	12.944
-5.0	-0.5	3.679	1.222	0.478	12.986
-5.0	-1.0	3.317	1.102	0.496	14.956
-5.0	-1.5	3.148	1.046	0.420	13.347
-5.0	-2.0	2.888	0.959	0.375	12.983
-5.0	-2.5	3.013	1.001	0.323	10.733
-5.0	-3.0	3.010	1.000	0.383	12.729
-5.0	-3.5	3.169	1.053	0.442	13.959
-5.0	-4.0	3.069	1.020	0.541	17.636
-5.0	-4.5	3.205	1.065	0.318	9.909
-5.0	-5.0	3.085	1.025	0.151	4.880
-5.0	-5.5	3.035	1.008	0.106	3.499
-5.0	-6.0	3.030	1.007	0.037	1.225
-5.0	-6.5	3.030	1.007	0.045	1.480
-5.0	-7.0	3.021	1.004	0.021	0.708
-5.0	-7.5	3.009	1.000	0.023	0.759
	U ∞ =	3.010			

LIST OF REFERENCES

1. Barlow, J.; Rae, W. Jr.; and Pope, A. Low Speed Wind Tunnel Testing 3rd ed. Wiley, New York, 1999.
2. Bradshaw, C. "An Experimental Investigation of Flapping Wing Aerodynamics in Micro Air Vehicles." Naval Postgraduate School: June 2003.
3. Kincaid, T. "Study of Micro-Sized Technology, Micro Air Vehicles, and Design of a Payload Carrying Flapping Wing Micro Air Vehicle." Naval Postgraduate School: March 2006.
4. Papadopoulos, J. "An Experimental Investigation of the Geometric Characteristics of Flapping Wing Propulsion for a Micro Air Vehicle." Naval Postgraduate School: March 2003.
5. Jones, K.D., and Platzer, M.F. "Experimental Investigation of the Aerodynamic Characteristics of Flapping-Wing Micro Air Vehicles," AIAA Paper No. 2003- 0418, Reno, Nevada, January 2003.
6. McMichael, J.M., and Francis, M.S. "Micro Air Vehicles – Toward a New Dimension in Flight." DARPA, USA, 1997.
7. Leith, J.; Raether, A.; and Smith, D. "Wind Tunnel Facility for Operation at Very Low Velocity."
8. Mehta, R., and Bradshaw, P. "Design Rules for Small Low Speed Wind Tunnels." Aeronautical Journal, November 1979.
9. Bell, J., and Mehta, R. "Boundary Layer Predictions for Small Low Speed Contractions." AIAA Journal, March 1989.
10. Jorgenson, F. "How to Measure Turbulence with Hot Wire Anemometers." Dantec Dynamics, 2004.
11. Prandtl, L. "Attaining a Steady Stream in Wind Tunnels." NACA TM 726, October 1933.

12. Schieman, J. "Comparison of Experimental and Theoretical Turbulence Reduction Characteristics for Screens, Honeycomb, and Honeycomb-Screen Combinations." NASA Technical Paper 1958, 1981.

13. Jones, K.; Bradshaw, C.; and Papadopoulos, J. "Improved performance and Control of Flapping Wing Propelled Micro Air Vehicles." AIAA Paper No. 2004-399, Reno, Nevada, January 2004.

14. Brassard, D. "Transformation of a Polynomial for a Contraction Wall Profile." February 2003.

15. Jones, K.; Duggan, S.; and Platzer, M. "Flapping Wing Propulsion for a Micro Air Vehicle." AIAA Paper No. 2001-0126, Reno, Nevada, January 2001.

INITIAL DISTRIBUTION LIST

1. Defense Technical Information Center
Ft. Belvoir, Virginia
2. Dudley Knox Library
Naval Postgraduate School
Monterey, California
3. Professor Kevin Jones
Naval Postgraduate School
Monterey, California
4. Professor Garth Hobson
Naval Postgraduate School
Monterey, California
5. LCDR Curt Hickle
Naval Postgraduate School
Monterey, California